Petroleum and Coal

**Article** **Open Access**

# A Hybrid Surrogate Intelligence Framework for Predictive Modelling and Proactive Optimisation of Wax Deposition in Crude Oil Flow Systems

*Buki Robert Oladele, Azunna I.B Ekejiuba, Angela Nkechi Nwachukwu, Stanley Toochukwu Ekwueme*

*Department of Petroleum Engineering, FUTO Owerri, Nigeria*

Received October 28, 2025; Accepted January 21, 2026

**Abstract**

This study presents a hybrid surrogate intelligence framework for the predictive modeling and optimization of wax deposition in crude oil flow systems. A comprehensive experimental dataset was generated from flow loop and cold finger tests to capture the interdependent effects of thermodynamic, hydrodynamic, and compositional parameters—namely flow velocity, pressure, temperature difference, wax appearance temperature, wax content, oil viscosity, and asphaltene concentration—on wax layer thickness. Two surrogate modeling techniques were developed and comparatively evaluated: Response Surface Methodology (RSM) employing a Custom Design matrix, and Artificial Neural Networks (ANN) trained using Levenberg–Marquardt (MLP-LM) and Bayesian Regularization (MLP-BR) algorithms. The RSM model facilitated parametric interpretation and statistical sensitivity analysis, while the ANN models provided high-fidelity nonlinear prediction capabilities. Optimization was achieved through RSM integrated with desirability functions (RSM-DF) and ANN coupled with a Genetic Algorithm (ANN-GA). The ANN-GA approach, particularly the MLP-BR-GA configuration, demonstrated superior performance, yielding a minimum predicted wax thickness of 0.223 mm compared to 0.385 mm from the RSM-DF model. Statistical evaluation confirmed the dominance of the MLP-BR architecture, with $R^2$ = 0.9918, RMSE = 0.3275, and MAPE = 0.1236, underscoring its robustness and generalization ability. The results reveal that optimal flow assurance conditions are achieved under low-pressure (~3 MPa), moderate temperature gradients (~5 °C), and reduced oil viscosity (~2.4 cP). Overall, the hybrid ANN-GA framework outperforms classical RSM-based techniques in accuracy and adaptability, establishing an effective data-driven paradigm for proactive wax management in crude oil production systems.

***Keywords:*** *Wax deposition; Artificial Neural Network; Response Surface Methodology; Genetic Algorithm; Flow assurance.*

## 1. Introduction

Wax deposition is among the most persistent and costly flow assurance challenges in crude oil production, particularly in deep onshore and offshore environments where ambient conditions promote the precipitation of paraffinic hydrocarbons from the produced crude. As the crude oil flows from the reservoir to the surface, its temperature decreases due to heat losses to the surrounding formation, casing, or seabed. When this temperature drops below the wax appearance temperature (WAT), the solubility of long-chain paraffin components—typically C18 to C36 alkanes—diminishes, leading to the nucleation and crystallization of solid wax. These wax crystals adhere to each other and to the pipe wall, forming a coherent and viscous layer that gradually thickens over time [1-2]. The deposit reduces the effective internal diameter of the tubing, increases pressure drop, decreases flow rate, and, in extreme cases, results in total plugging of the wellbore or flowline. Such outcomes cause production deferment, operational downtime, and significant economic losses due to the frequent need for cleaning, intervention, or well shut-in [3-4].

The phenomenon of wax deposition is controlled by a combination of thermodynamic, hydrodynamic , and compositional factors. Thermodynamically, wax formation begins when the between the liquid and solid phases of paraffinic components is disturbed, and the temperature at which this occurs defines the WAT [5]. Below this temperature, solid wax crystals form and begin to separate from the liquid phase. Hydrodynamic factors, including flow velocity, shear rate, and turbulence intensity, influence the extent of deposition, as they govern the balance between deposition and removal mechanisms [1-2]. Under high-velocity turbulent flow, shear forces tend to prevent excessive buildup by promoting re-entrainment of crystals back into the flow stream, while in laminar or low-velocity regimes, deposition dominates due to insufficient shear. Compositional factors such as crude oil wax content, resin-to-asphaltene ratio, and viscosity determine the nature and strength of the wax network that forms [6]. Oils rich in high-molecular-weight paraffins tend to form stronger crystalline networks that trap large amounts of liquid, resulting in gel formation and severe flow restriction [7].

The mechanism of wax deposition is inherently complex because it involves coupled heat, mass, and momentum transfer phenomena. Initially, molecular diffusion is the dominant mechanism, as dissolved wax molecules migrate from the warmer core of the flow to the colder pipe wall driven by a concentration gradient. As the temperature difference between the bulk oil and the wall increases, the diffusion flux intensifies, causing accelerated deposition [4]. Once a layer of wax forms, it acts as an insulating barrier, further decreasing the wall temperature and promoting more precipitation. The deposit thickens until a steady-state condition is achieved, where the rate of deposition equals the rate of shear removal. However, variations in production rate, temperature, or composition continuously disturb this equilibrium, resulting in cyclic deposition and removal behavior [1]. Other contributing mechanisms include Brownian motion of small crystals, shear dispersion that enhances particle transport, and gravitational settling of heavier wax particles, especially in inclined or horizontal wells [8].

The formation of wax deposits adversely affects production efficiency and equipment integrity. The reduced flow area increases pressure losses and elevates the load on artificial lift systems such as electrical submersible pumps (ESPs) or gas-lift valves. The increased power demand can lead to premature pump failures or gas-lift instability [9]. In subsea systems, where maintenance access is limited, wax plugging can lead to prolonged downtime and costly remediation operations using remotely operated vehicles (ROVs) or pigging units [3]. The economic implications are profound, as de-waxing activities—whether thermal, mechanical, or chemical—require substantial investment. Moreover, the recurrence of wax deposition in wells that are frequently shut-in or experience transient flow conditions creates a recurring cost burden, often running into millions of dollars annually for large offshore operations [2].

The available mitigation and remediation strategies for wax deposition can broadly be classified into thermal, mechanical, and chemical approaches. Thermal techniques, such as hot oiling and hot water circulation, are the most commonly employed. They involve pumping heated fluids into the wellbore to melt the deposited wax and restore flow capacity [3]. Although effective, these operations are energy-intensive, transient in effect, and can cause scaling or thermal fatigue of the tubing. Mechanical methods, including pigging, wireline scraping, and coiled tubing milling, physically remove the deposits but necessitate well shut-ins, which lead to production interruptions. In subsea and deviated wells, mechanical cleaning becomes operationally difficult and risky [1]. Chemical methods employ solvents, dispersants, or paraffin inhibitors that alter the crystallization behavior of wax molecules [6]. While these can delay deposition, their performance is strongly dependent on crude composition and environmental conditions. Furthermore, chemical treatments require continuous injection and monitoring, increasing operational complexity. These existing methods, although mature, share a critical limitation—they are reactive rather than proactive. Most de-waxing interventions are carried out after measurable production decline or pressure anomalies, by which time wax deposition has already impaired flow [10]. This reactive operational mode results in excessive maintenance frequency, high energy expenditure, and non-optimized use of resources.

Consequently, there has been a growing interest in predictive and preventive control strategies that rely on real-time data analysis and forecasting. The ability to predict when and

where wax will deposit within the production system can enable timely and optimized interventions, reducing downtime and improving cost efficiency [11]. Conventional predictive tools based on thermodynamic modeling and empirical correlations, however, have proven inadequate for practical field application. Thermodynamic models such as regular solution theory and solid solution models require extensive compositional data for each hydrocarbon component, which are rarely available [1]. They also assume equilibrium conditions, neglecting the transient effects of flow rate and temperature fluctuations. Empirical correlations, on the other hand, are derived under limited laboratory conditions and lack generalization capability when applied to diverse field environments. The multiphysics nature of wax deposition, with its strong nonlinear dependencies on temperature, pressure, flow regime, and crude composition, challenges the applicability of these classical methods [2].

Recent advances in data science and artificial intelligence (AI) have opened new possibilities for addressing such nonlinear, multivariate flow assurance problems through data-driven modeling. Machine learning (ML) approaches, in particular, offer powerful tools for pattern recognition, feature selection, and predictive modeling without requiring explicit physical equations [7,9]. By learning directly from historical and real-time production data, ML algorithms can infer hidden relationships between operational parameters and wax deposition outcomes. Algorithms such as Artificial Neural Networks (ANN), Support Vector Machines (SVM), Random Forests (RF), and Gradient Boosting Decision Trees (GBDT) have been successfully applied to analogous problems such as hydrate formation prediction, asphaltene precipitation, and corrosion rate forecasting [12-13]. These successes suggest a strong potential for machine learning to revolutionize wax deposition forecasting and intervention optimization in oil production systems.

Among these techniques, the Artificial Neural Network (ANN) stands out due to its ability to capture highly nonlinear interactions between multiple inputs and outputs [11]. ANNs mimic the human brain's learning process by adjusting the connection weights between neurons based on training data, enabling them to predict complex responses even under noisy and incomplete datasets. For wax deposition modeling, ANN can be trained using operational parameters such as flow rate, tubing pressure, temperature profile, oil viscosity, and wax appearance temperature to predict outputs such as wax layer thickness or deposition rate [13]. The model learns from historical data trends to forecast future deposition behavior under varying conditions. This predictive capability can be further extended by integrating the ANN model with optimization algorithms that recommend the most efficient and cost-effective dewaxing schedules based on predicted outcomes [2].

Despite these possibilities, the application of machine learning to wax deposition forecasting remains in its infancy, and several research gaps persist. Most existing studies focus on steady-state or laboratory-scale systems, using limited datasets and static variables [1]. Very few have addressed the transient and dynamic nature of wax deposition under real field conditions where parameters vary continuously. Furthermore, previous models have primarily targeted prediction alone, neglecting the operational decision-making aspect of when and how to intervene. There is also a scarcity of models that generalize well across different wells and crude oil types, as most machine learning implementations remain case-specific. Data-driven models for wax deposition must also contend with challenges such as sparse datasets, variable sampling frequencies, and the need for feature normalization, which have not been adequately explored in earlier works [9,11]. Consequently, there is a clear need for a robust and generalizable predictive framework that integrates machine learning-based forecasting with optimization of intervention strategies, using readily available production data.

Response Surface Methodology (RSM) represents another powerful surrogate modeling approach widely applied in process optimization and prediction. RSM combines statistical and mathematical techniques to model and analyze the relationships between multiple input variables and one or more output responses. It is particularly effective for developing empirical correlations and identifying optimal operating conditions with a relatively small number of experimental runs. For wax deposition studies, RSM can be employed to quantify the combined effects of parameters such as flow velocity, pressure, temperature gradient, and crude oil composition on wax thickness or deposition rate, while generating response surfaces that

facilitate visualization and optimization of the process behavior [14]. When used alongside ANN, RSM serves as a complementary tool — offering interpretability and analytical precision that can validate or cross-check the results of data-driven models.

Despite these possibilities, the application of both machine learning and statistical surrogate modeling to wax deposition forecasting remains in its infancy, and several research gaps persist. Most existing studies focus on steady-state or laboratory-scale systems using limited datasets and static variables [1]. Very few have addressed the transient and dynamic nature of wax deposition under real field conditions where parameters vary continuously. Furthermore, previous models have primarily targeted prediction alone, neglecting the operational decision-making aspect of when and how to intervene. There is also a scarcity of models that generalize well across different wells and crude oil types, as most machine learning and RSM implementations remain case-specific. Data-driven models for wax deposition must also contend with challenges such as sparse datasets, variable sampling frequencies, and the need for feature normalization, which have not been adequately explored in earlier works [9,11]. Consequently, there is a clear need for a robust and generalizable predictive framework that integrates both machine learning–based forecasting and statistical optimization techniques such as RSM to develop reliable models and optimize intervention strategies using readily available production data.

This study presents a novel hybrid data-driven framework that addresses the longstanding challenge of developing a predictive and adaptive system for anticipating wax deposition and optimizing de-waxing operations in crude oil production systems. Traditional mechanistic and empirical models remain constrained by their deterministic formulations, reliance on detailed compositional data, and limited adaptability to dynamic field variations. Current operational practices—often reactive and schedule-based—lead to suboptimal wax management, resulting in increased downtime, higher maintenance costs, and reduced production efficiency. To overcome these limitations, the present research introduces an integrated surrogate modeling framework that combines Artificial Neural Network (ANN) and Response Surface Methodology (RSM) approaches for both prediction and optimization of wax deposition phenomena. The framework employs multilayer perceptron (MLP) ANN architectures trained on comprehensive field-scale and experimental datasets encompassing thermodynamic, hydrodynamic, and compositional parameters such as flow velocity (Vf), pressure (P), temperature difference (ΔT), wax appearance temperature (TWAT), wax content (Wc), oil viscosity (μo), and asphaltene content (Ac). The MLP-ANN is implemented using two distinct training algorithms—the Levenberg–Marquardt (LM) and Bayesian Regularization (BR)—to assess comparative performance in terms of generalization capability and prediction accuracy.

Furthermore, an RSM-based model is developed using a custom experimental design matrix to establish empirical relationships between the input variables and the output parameter, wax thickness (δw). This statistical model facilitates visualization of the response surfaces and interaction effects among parameters, offering interpretability that complements the data-driven ANN approach. For optimization, two independent strategies are employed: the ANN-GA (Genetic Algorithm coupled with ANN) framework, which leverages the ANN's nonlinear predictive power within an evolutionary optimization scheme to identify optimal de-waxing schedules and operating conditions; and the RSM-DF (RSM with Desirability Function) method, which simultaneously maximizes or minimizes multiple response targets based on defined desirability criteria. A comparative evaluation is conducted between the ANN-based and RSM-based models for both modelling accuracy and optimization efficiency, using statistical metrics such as $R^2$, RMSE, MAE, and MAPE. This dual-modelling strategy enables cross-validation of predictive robustness and optimization performance.

## 2. Surrogate modelling of wax deposition

Surrogate modelling has emerged as a powerful alternative to mechanistic and purely empirical approaches for predicting wax deposition in crude oil transport systems. These data-driven or semi-empirical models approximate the underlying physics using statistical and machine learning methods, enabling rapid prediction and optimisation with reduced

computational cost. Among the most widely applied surrogate techniques are the Artificial Neural Network (ANN) and the Response Surface Methodology (RSM).

### 2.1. Artificial Neural Networks (ANNs)

ANNs have emerged as powerful computational modeling tools for addressing complex non-linear relationships in petroleum production systems, particularly in the prediction and control of wax deposition phenomena in oil pipelines and wellbores [15]. Wax deposition is a highly nonlinear process influenced by multiple interacting parameters such as flow velocity, system pressure, temperature gradient (ΔT), wax appearance temperature (WAT), wax content, oil viscosity, and asphaltene concentration, all of which collectively govern wax precipitation, crystal growth, and deposition thickness. Traditional empirical or mechanistic models often fail to accurately capture these intricate relationships due to uncertainties in flow dynamics and thermodynamic conditions. In contrast, ANNs provide a robust data-driven framework capable of learning and modeling these dependencies directly from experimental or field data [16].

An ANN structured as an interconnected network of artificial neurons organized in layers, consisting of an input layer, one or more hidden layers, and an output layer, represents a Multilayer Perceptron (MLP) architecture, which is a type of feedforward neural network (FFNN). In this configuration, data flows in a single direction from the input layer through the hidden layers to the output layer without any feedback connections [17]. Each neuron processes the incoming signals through weighted connections, applies an activation function to introduce nonlinearity, and passes the transformed signal to the next layer. The network is typically trained using the backpropagation (BPNN) algorithm, which iteratively updates the connection weights based on the difference between the predicted and target outputs, minimizing this error through gradient descent or advanced optimization techniques such as the Levenberg–Marquardt (LM) or Bayesian Regularization (BR) algorithms. For example, in wax deposition modeling, the input neurons represent key operational and fluid parameters such as flow velocity (V), pressure (P), temperature difference (ΔT), wax appearance temperature (WAT), wax content (WC), oil viscosity (μo), and asphaltene content (AC), while the output neuron corresponds to the predicted wax layer thickness (Wt) under specific flow and thermal conditions [18].

Mathematically, the output of the *n*th neuron in the input or hidden layer is expressed as the weighted sum of all input signals plus a bias term, formulated as:

$$z_n = \left(\sum_{i=1}^{k} w_{ij}\, x_i\right) + b_n \qquad (1)$$

where $z_n$ is the net input to the *n*th neuron; $w_{ij}$ represents the connection weight between the *i*th input and the *n*th neuron; $x_i$ denotes the *i*th input variable; $b_n$ is the bias associated with the neuron; and mmm is the total number of inputs. This weighted summation serves as the neuron's internal activation potential, which is then passed through an activation (or transfer) function to generate the neuron's output response.

The transfer (activation) function then transforms $z_n$ into a nonlinear output signal $f_n$, defined as:

$$f_n = f(z_n) \qquad (2)$$

Different transfer (activation) functions can be used depending on the level of nonlinearity present in the modeled system. In wax deposition modeling, which involves complex thermo-hydraulic and compositional nonlinear interactions, the tangent sigmoid (tansig), log-sigmoid (logsig), and pure linear (purelin) functions are widely adopted because of their smooth differentiability and their capability to represent nonlinear mappings during training. These functions are mathematically expressed as follows.

For tangent sigmoid:

$$f(x) = \frac{2}{1 + e^{-2z}} - 1 \qquad (3)$$

For Log-sigmoid

$$f(x) = \frac{1}{1+e^{-z}} \qquad (4)$$

For pureline:

$$f(z) = z \quad (5)$$

The selection of these activation functions depends on the data normalization method: tansig is best suited for inputs normalized within the range of −1 to 1, logsig works effectively for data scaled between 0 and 1, and purelin is typically applied in the output layer for regression problems where a linear relationship between the processed signals and the output is anticipated. The hidden layer neurons compute nonlinear transformations of the inputs, thereby capturing intricate dependencies among the parameters affecting wax deposition [15]. The output of each hidden layer neuron $h_j$ is thus given by:

$$h_j = f_h\left(\sum_{i=1}^{k} w_{ij}\, x_i\right) + b_j \quad (6)$$

where $f_h$ denotes the activation function (typically tansig or logsig); and $w_{ij}$ represents the weight between input neuron i and hidden neuron j. The output neuron aggregates the transformed signals from the hidden layer and applies an output transfer function, often linear for regression tasks such as wax thickness prediction: $\hat{y} = f_o\left(\sum_{i=1}^{k} w_{jo}\, x_i\right) + b_o$

where $f_o$ is the output activation function (commonly purelin); $w_{jo}$ is the weight connecting hidden neuron j to the output neuron; and ŷ represents the network-predicted wax thickness.

The training process iteratively adjusts all weights ($w_{ij}$, $w_{jo}$) and biases ($b_j$, $b_o$) to minimize the deviation between predicted and measured wax thickness values. The training of the ANN for wax deposition modeling is executed using numerical optimization algorithms designed to minimize a loss (error) function, typically defined as the Mean Squared Error (MSE):

$$E = \frac{1}{2N}\sum_{p=1}^{N}\left(y_p - \hat{y}_p\right)^2 \quad (8)$$

where $y_p$ is the actual measured wax thickness; $\hat{y}_p$ is the ANN-predicted value; and N is the number of training samples.

The Levenberg–Marquardt (LM) algorithm is one of the most efficient training methods for nonlinear process models such as wax deposition. It combines the speed of the Gauss–Newton algorithm with the stability of gradient descent, making it particularly effective for medium-sized networks with smooth error surfaces. The LM algorithm minimizes the cost function by adjusting weights according to:

$$[\Delta w = -(J^{\mathrm{T}}J + \lambda I)^{-1}J^{\mathrm{T}}e] \quad (9)$$

where J is the Jacobian matrix of partial derivatives of the network errors with respect to weights; I is the identity matrix; λ is the damping factor; and e = y - ŷ represents the error vector between measured and predicted wax thickness values.

The Jacobian matrix J is expressed as:

$$J = \frac{\partial e}{\partial w} \quad (10)$$

The weight update rule is then:

$$w^{(k+1)} = w^{(k)} + \Delta w \quad (11)$$

The damping factor (λ) in the Levenberg–Marquardt (LM) algorithm is dynamically adjusted during the training process—decreasing when the model's performance improves and increasing when the prediction error grows. This adaptive control enables a seamless transition between the Gauss–Newton method, which offers rapid convergence near the optimal solution, and gradient descent, which provides stability when the system is far from the minimum. Consequently, the LM algorithm delivers highly efficient convergence for nonlinear modeling tasks such as wax deposition prediction, where the relationships between process variables are complex, multivariate, and data-dependent [19].

In contrast, the Bayesian Regularization (BR) method incorporates probabilistic regularization to enhance model generalization and mitigate overfitting—an essential consideration in wax deposition studies where available training data are often sparse or affected by measurement noise. BR modifies the conventional error function by adding a regularization term that penalizes large network weights, thus favoring smoother mappings and reducing sensitivity to

outliers. This balance between model accuracy and complexity allows BR-trained networks to maintain predictive robustness across varying flow, thermal, and compositional conditions encountered in pipeline wax deposition modeling.

$$E = E_D + \alpha E_W \quad (12)$$

where: $E_D$ is the data error term (mean squared error)

$$E_D = \frac{1}{2}\sum_{i=1}^{n}(y_i - \hat{y}_i)^2 \quad (13)$$

where, $y_i$is the target output; and $(\hat{y}_i)$ is the network output for the i-th training example.

$E_W$is the weight decay term (sum of squares of the weights)

$$E_W = \frac{1}{2}\sum_{j=1}^{m} w_j^2 \quad (14)$$

where, $(w_j$ represents the weights of the network; and $\alpha$ is the regularization parameter that governs the balance between accurately fitting the training data and minimizing the magnitude of the network weights.

During the training process, Bayesian Regularization (BR) automatically adjusts $\alpha$ and other related hyperparameters to maximize the model evidence, thereby identifying the simplest ANN architecture that can effectively represent the wax deposition behavior. Through this adaptive mechanism, the BR-trained ANN achieves enhanced robustness and generalization capability, allowing it to accurately predict wax layer thickness across a wide range of operating conditions, even when the available data are sparse or noisy [20]. This characteristic is particularly valuable in field-scale wax deposition modeling, where variations in crude composition, flow velocity, and temperature gradients are prevalent, and many mechanistic parameters cannot be directly measured or validated experimentally.

Several studies have employed artificial neural-networks (ANNs) to model wax deposition phenomena with promising accuracy but varying methodological limitations. For example, Xie & Xing [19] used a radial-basis-function neural network (RBF-NN) to predict wax-deposition rate in crude-oil pipelines based on four key influencing factors; they achieved strong fit metrics though the dataset was small and lacked field-scale validation. Jalalnezhad & Kamali [21] developed an adaptive-network-based fuzzy inference system (ANFIS, hybrid of fuzzy logic + ANN) to predict wax deposition thickness under single-phase turbulent flow conditions, reporting excellent R (0.9929) and low deviation error (~0.0157) but faced limitations around narrow input conditions and lack of multiphase flow generalisation. Chen [22] applied a feed-forward ANN to model wax deposition rate for waxy crude oil pipelines, integrating experimental data and achieving low average relative error; yet the study still lacked development of a mechanistic linkage to asphaltene interactions and pressure effects. Kim *et al.* [23] proposed an AI-based model (including ANN elements) to predict both the location and amount of wax in oil pipelines using sensor and experimental inputs, showing good agreement with laboratory/field data but being constrained by limited oil types and pipe geometries. Jin et al. [24] developed a machine-learning based ANN model to predict wax deposition thickness on pipe walls from experimental loop data, achieving very low error metrics but still confronted limitations tied to dataset size and uncertain field transferability. Obaseki *et al.* [25] used dynamic modelling to predict wax deposition in pipelines, incorporating ANN elements alongside dynamic simulation, highlighting the nonlinear behaviour of deposition but showing that transient multiphase effects were not fully captured.

### 2.2. Response surface methodology

Response Surface Methodology (RSM) is a systematic and efficient suite of statistical and mathematical techniques for building empirical models of a response (output) as a function of several input (factor) variables, and for using those models to explore, visualize and optimize the response. In the context of wax deposition modelling - where the response of interest is wax thickness and the key input factors are flow velocity (m/s), pressure (MPa), ΔT (°C), WAT (°C), wax content (% wt), oil viscosity (cP) and asphaltene content (% wt). RSM offers a

pragmatic way to replace costly or time-consuming physical experiments by a fitted polynomial model that captures main, interaction and curvature effects, and then to use that model for prediction, sensitivity analysis and optimization of operating conditions to reduce wax build-up [26].

The standard RSM workflow begins with experimental design. For seven continuous factors a full two-level factorial design ($2^7$ runs) would be exhaustive but often impractical; therefore, practitioners typically use fractional factorials to screen for important factors, followed by a second-order design centered on the active factors. Common second-order designs are the Central Composite Design (CCD) and the Box–Behnken Design (BBD). A CCD for k factors typically consists of a $2^k$ factorial or fractional factorial portion, 2k axial ("star") points at levels ±α for each factor to enable estimation of curvature, and several replicates at the design center to estimate pure error. Levels are usually coded to scaled variables xi where xi=Xi−X0,i )/Δi, with X0,i the center point and Δi the half-range so that coded levels are conveniently comparable across factors.

With the experimental design in place, the experiments are conducted by systematically varying the input factors according to the selected design matrix. For each combination of factor levels, the corresponding wax thickness is measured and recorded. Maintaining consistency, accuracy, and precision in data collection at this stage is essential to ensure the reliability and statistical validity of the results. For example, different combinations of flow velocity, system pressure, temperature differential (ΔT), wax appearance temperature (WAT), wax content, oil viscosity, and asphaltene content are tested, and the corresponding wax deposition thicknesses are obtained [26]. This provides the data foundation for developing a predictive and optimization model for wax formation under varying production and thermal conditions.

The next step involves constructing a mathematical model that quantitatively describes the relationship between the selected input factors and the response variable—wax thickness. In RSM, this is typically achieved by fitting the experimental data to a polynomial regression model that approximates the underlying physical relationship between the parameters. The models generally include linear, interaction (two-factor interaction, 2FI), and quadratic terms to capture both main and combined effects [27]. The general form of the models for linear regression is given as

$$y = a_o + \sum_{i=1}^{k} a_i x_i + e \qquad (15)$$

The general form of the 2FI regression model is given as

$$y = a_o + \sum_{i=1}^{k} a_i x_i + \sum_{i<j}^{k} a_{ij} x_i x_j + e \qquad (16)$$

The general form of the quadratic regression model is given as

$$y = a_o + \sum_{i=1}^{k} a_i x_i + \sum_{i<j}^{k} a_{ij} x_i x_j + \sum_{i=1}^{k} a_{ii} x_i^2 + e \qquad (17)$$

where $x_i$,$x_j$, $x_l$, are the input variables and $a_i$, $a_{ij}$, $a_{ii}$,and $a_{ijl}$ are the coefficient of each of the terms, $a_o$ is the offset and e is the residual or error term.

The coefficients are estimated using regression analysis techniques, typically through the least squares method implemented in statistical software such as Design-Expert, Minitab, or MATLAB. The fitted polynomial model thus serves as a surrogate empirical representation of wax deposition behavior.

Following model development, statistical analysis is performed to evaluate the adequacy, validity, and reliability of the regression model. The most important analytical tool in this context is Analysis of Variance (ANOVA). ANOVA is used to assess both the overall significance of the developed regression model and the individual influence of each factor and interaction term on wax thickness. It decomposes the total variability of the response into components attributable to the model and to residual (unexplained) error. A small *p*-value (typically <

0.05) indicates that the regression model or an individual factor is statistically significant in influencing wax formation [27]. ANOVA also reveals significant interaction effects—for example, how the combined effect of flow velocity and ΔT influences the rate or thickness of wax deposition, which may differ from their individual contributions.

In addition to ANOVA, the estimated regression coefficients are statistically tested to determine their significance and contribution to the model. Each coefficient reflects the magnitude and direction of the relationship between its corresponding factor and the response. The linear terms describe direct effects (e.g., increasing flow velocity may reduce wax thickness), the interaction terms capture coupled effects (e.g., the combined influence of viscosity and WAT), and the quadratic terms represent curvature effects in the response surface [26]. These fitted terms allow the quadratic RSM model to accurately reproduce the nonlinear behavior typically observed in wax deposition phenomena.

Once the model has been statistically validated, its adequacy is further verified through model diagnostic checks. Important statistical indicators include the coefficient of determination ($R^2$), the adjusted $R^2$, and the predicted $R^2$. The $R^2$ value indicates the proportion of the total variation in wax thickness that is explained by the model, while the adjusted $R^2$ corrects for the number of predictors included, penalizing overfitting. Additionally, a lack-of-fit test is performed to determine whether the fitted model sufficiently captures the experimental data trends. A non-significant lack-of-fit ($p > 0.05$) confirms that the model is appropriate within the tested region. Residual analysis is also conducted to verify model assumptions; the residuals (differences between observed and predicted wax thickness values) should be randomly distributed and approximately normal. If residuals show systematic patterns, the model may need refinement, such as transformation or inclusion of additional terms.

After the model adequacy is confirmed, response surface and contour plots are generated to visualize the relationships between key factors and wax deposition. These graphical tools provide an intuitive means of understanding the interaction between two variables while holding others constant. A 3D response surface plot shows how the wax thickness changes as two factors vary, revealing peaks or valleys that correspond to maximum or minimum deposition. For instance, increasing flow velocity and decreasing ΔT may jointly minimize wax deposition, reflecting the dominance of shear-induced wax removal at high turbulence. Contour plots, which are 2D projections of the response surfaces, depict lines of constant wax thickness and are valuable for identifying operational regions that yield minimal wax buildup [27-28].

Once the response surfaces are established, optimization is performed to identify the factor settings that achieve the desired response objective—typically, minimizing wax thickness. The optimization can be carried out using either analytical or numerical approaches. In direct optimization, the polynomial regression model is solved to find the stationary point (minimum or maximum) of the response surface. Alternatively, desirability analysis can be used, especially when multiple performance objectives must be balanced, such as minimizing wax deposition while maintaining acceptable flow velocity and pressure drop. In this approach, each response is assigned a desirability function ranging from 0 (undesirable) to 1 (fully desirable), and the overall desirability function is maximized to identify optimal conditions that represent the best trade-off among competing criteria [26].

The final stage of the RSM-based modeling process is model validation. This involves conducting additional experiments at the predicted optimal levels of the input factors to verify the accuracy of the model's predictions. For wax deposition modeling, the predicted wax thickness at optimal operating conditions is compared to experimental measurements obtained under the same conditions. A close agreement between the predicted and observed values confirms that the developed RSM model is both valid and reliable. Conversely, significant deviations may indicate the need for model refinement, possibly by expanding the experimental domain or incorporating higher-order effects [27]. This validation step is crucial for ensuring confidence in the model's predictive capability and its applicability for real-field operations.

Through this systematic RSM framework, wax deposition behavior can be quantitatively modeled and optimized based on measurable operational and compositional parameters. The approach enables identification of the most influential factors—such as ΔT, flow velocity, and

wax content—and their synergistic effects on deposition dynamics. More importantly, it allows for determination of the optimal operational window that minimizes wax buildup, thereby improving flow assurance and reducing maintenance costs in oil production systems [28].

Ridzuan *et al.* [14] applied Response Surface Methodology (RSM) using a rotatable Central Composite Design (CCD) to optimize wax deposition measured with a cold-finger apparatus; they treated cold-finger temperature and experimental duration as the two coded factors, fitted a second-order polynomial (after a log transformation) and used ANOVA to validate the model, reporting the fitted model ln(wax deposit+0.02) = −0.19 + 0.15B − 1.03A − 7.338e−03 AB + 0.033B² − 0.35A² and showing excellent agreement between predicted and observed values with a verified minimum wax deposit of 0.0042 g at the optimized conditions; their study demonstrates RSM's strength for efficient experimental reduction and sensitivity analysis but is limited by the two-factor scope (so interactions with other operational variables like flow or composition were not examined) and by cold-finger lab conditions that reduce direct field transferability.

Salam, *et al.* [29] investigated paraffin-wax deposition in pipeline flow by screening and then modelling key operating parameters (temperature differential, flowrate and residence time) with a Box–Behnken RSM design to develop a quadratic regression surrogate; their ANOVA and model diagnostics returned strong predictive statistics (Pred $R^2 \approx 0.9618$ and Adj $R^2 \approx 0.9945$) and the model predicted a minimum wax deposit of 0.0195075 g at temperature = 53.25 °C, flowrate = 499.54 mL/min and residence time = 3.01 min, demonstrating that temperature, time and certain squared and interaction terms dominate deposition behavior; the work's main contribution is a validated empirical model usable to navigate the design space for mitigation, while its limitations include confinement to the tested ranges, reliance on laboratory flow rigs (limiting multiphase and large-scale applicability) and omission of compositional complexities that occur in real crude systems.

Adeyanju and Oyekunle [30]. used a fabricated flow-loop rig to study wax deposition in subcooled pipeline conditions and applied Central Composite Design (CCD) RSM to quantify main and interaction effects of wall (coolant) temperature, inlet oil temperature, wax inhibitor concentration and oil flowrate on deposit volume; their model showed good fit between predicted and experimental values (predicted R-squares in reasonable agreement with adjusted $R^2$) and reported substantial reductions in deposit volumes across laminar and transition regimes (with predictive errors ~4–5%), enabling identification of significant terms (A, B, C, D and various interactions) for targeted mitigation; however, being a conference experimental study, limitations include restricted dataset size, specific crude/inhibitor types (which constrain generalisability), and the typical lab-to-field scaling uncertainty for pipeline systems.

Elganidi *et al.* [31] applied RSM (CCD) to optimise the synthesis parameters of a novel polymeric pour-point depressant/flow improver intended to control wax deposition, modelling the effect of reaction temperature, time and initiator concentration on polymerisation yield; their quadratic regression model produced $R^2 = 0.9696$ and identified optimal polymerisation conditions (reaction time ≈ 8.1 h, temperature ≈ 102 °C, initiator ≈ 1.57 wt%) that yielded a predicted maximum polymer yield of 93.75%, which experimental validation runs confirmed with an average yield of 93.20% (error ≈ 0.55%); while this study demonstrates how RSM can efficiently optimise wax-inhibitor production with strong statistical validation, limitations include that the study addresses additive synthesis rather than in-pipe deposition dynamics directly, and that the effectiveness of the synthesised polymer as a field inhibitor requires further flow-loop and field validation under diverse crude and thermal conditions.

## 3. Model simulation

In this study, both RSM and ANN models were employed as surrogate modeling tools to capture and predict the complex nonlinear behavior of wax deposition under varying flow and thermodynamic conditions. Surrogate models serve as efficient mathematical approximations of experimentally observed systems, enabling rapid prediction and optimization without requiring extensive laboratory or field testing. The RSM model provided an interpretable, statistically driven framework capable of describing quadratic relationships among the seven input

factors, while the ANN model offered superior flexibility in learning nonlinear and multidimensional interactions that govern wax formation and growth. By integrating these two complementary modeling techniques, the study established reliable predictive relationships between the input parameters—flow velocity (Vf), pressure (P), temperature difference (ΔT), wax appearance temperature (TWAT), wax content (Wc), oil viscosity (μo), and asphaltene content (Ac)—and the response variable, wax thickness (δw). The use of RSM and ANN as surrogate models thus provided a comprehensive and computationally efficient approach for understanding, predicting, and optimizing wax deposition behavior in pipeline flow systems.

### 3.1. Data preparation

A comprehensive experimental dataset was developed to establish and validate the proposed wax deposition prediction models. The database consists of 150 experimental observations obtained from a series of controlled flow loop and cold finger experiments, designed to simulate wax deposition under representative pipeline operating conditions. In these experiments, a synthetic crude oil system of known composition was circulated through a temperature-controlled stainless steel flow loop, enabling precise control of flow velocity, pressure, and temperature gradient between the bulk fluid and pipe wall. The extent of wax deposition was quantified by periodically measuring the wax layer thickness (δw, mm) on the inner pipe surface using laser micrometry and gravimetric analysis, following procedures similar to those recommended in standard flow assurance testing protocols.

The selected input parameters encompass the major thermophysical and compositional factors governing wax precipitation and growth dynamics. These include flow velocity (Vf, m/s), pressure (P, MPa), temperature difference (ΔT, °C) between bulk oil and wall surface, wax appearance temperature (TWAT, °C), wax content (Wc, %), oil viscosity (μo, cP), and asphaltene content (Ac, %). Each experiment was conducted under steady-state conditions to ensure reliable measurements of deposition thickness. The output variable, wax thickness (δw, mm), represents the overall measure of deposition severity and is the primary response used for model development and optimization. The resulting dataset provides a robust basis for correlating the complex nonlinear relationships between the thermodynamic, rheological, and compositional properties of crude oil systems and the observed extent of wax deposition.

### 3.2. ANN modelling

ANN models were developed using MATLAB to predict the nonlinear relationship between the governing process variables and the extent of wax deposition. The experimental data obtained from the controlled flow loop and cold finger tests were used as the input dataset for the modeling. The ANN development and simulation were carried out using MATLAB's Neural Network Toolbox (nntool), which offers multiple training algorithms and transfer functions for optimizing predictive accuracy.

A feed-forward multilayer perceptron (MLP) network based on the backpropagation learning principle was adopted to model the complex interactions among the process parameters. Two training algorithms were implemented and compared: the Levenberg–Marquardt (LM, trainlm) and the Bayesian Regularization (BR, trainbr) methods. The LM algorithm was evaluated for its fast convergence and suitability for smaller datasets, while the BR algorithm was tested for its strong generalization capability and reduced risk of overfitting.

The network structure consisted of seven input neurons, representing flow velocity (Vf, m/s), pressure (P, MPa), temperature difference (ΔT, °C), wax appearance temperature (TWAT, °C), wax content (Wc, %), oil viscosity (μo, cP), and asphaltene content (Ac, %). A single output neuron corresponding to wax thickness (δw, mm) was used to capture the wax deposition response. The hidden layer employed a tangent sigmoid (TANSIG) transfer function to account for nonlinear relationships, while a pure linear (PURELIN) function was used at the output layer to ensure continuous-valued predictions.

Multiple network topologies with hidden neuron numbers ranging from 5 to 20 were examined to identify the configuration that produced the best prediction accuracy. The dataset was randomly divided into training (70%), validation (15%), and testing (15%) subsets to ensure

unbiased model evaluation. Model performance was assessed using statistical indicators including the correlation coefficient (R), coefficient of determination ($R^2$), mean squared error (MSE), root mean squared error (RMSE), mean absolute error (MAE), and mean absolute percentage error (MAPE). Figure 1 shows the topology of the ANN model

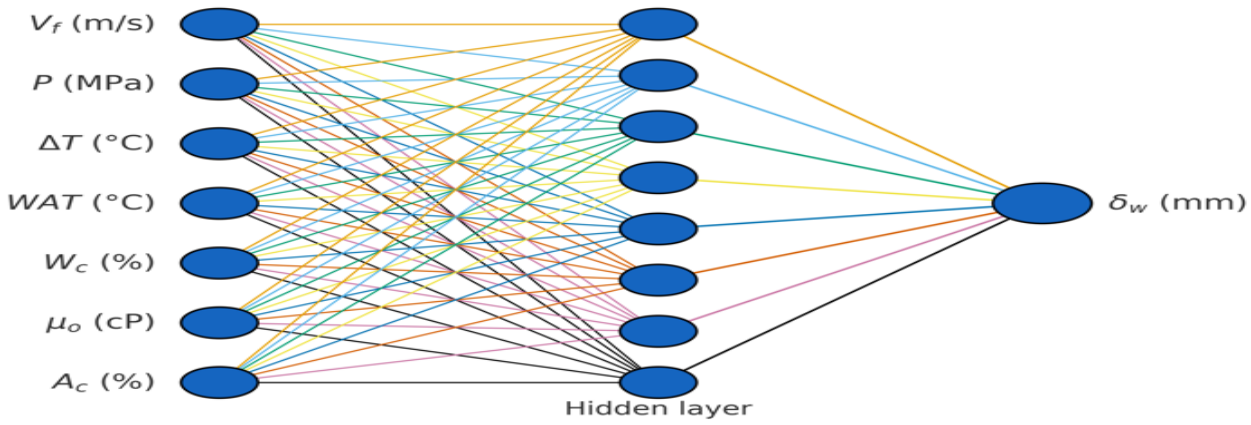


Figure 1. ANN topology for wax deposition.

### 3.3. RSM modelling

The experimental data obtained from the controlled flow loop and cold finger tests served as the foundation for the Response Surface Methodology (RSM) modeling of wax deposition. A Custom Design model was implemented using Design-Expert software (version 13) to establish quantitative relationships between the key input parameters and the wax thickness response. The custom design approach was adopted for this study due to its flexibility in accommodating non-standard experimental configurations and unequal factor levels, making it particularly suitable for complex flow assurance systems such as wax deposition processes.

Seven independent variables were considered as input factors: flow velocity (Vf, m/s), pressure (P, MPa), temperature difference (ΔT, °C), wax appearance temperature (TWAT, °C), wax content (Wc, %), oil viscosity (μo, cP), and asphaltene content (Ac, %). The wax thickness (δw, mm) was selected as the output response variable representing the extent of wax deposition under various operating conditions. The RSM model was generated based on experimentally measured data, and multiple regression models—including linear, two-factor interaction (2FI), and quadratic models—were evaluated to determine the most statistically significant representation of the experimental results. Model performance was assessed using statistical criteria such as the coefficient of determination ($R^2$), adjusted $R^2$, predicted $R^2$, standard deviation, and coefficient of variation (COV). Among these, the quadratic model provided the best fit for predicting wax thickness, effectively capturing the nonlinear interactions among the studied parameters. The final RSM model, developed through the Design-Expert platform, enabled the prediction and optimization of wax deposition behavior across the experimental domain.

### 3.4. Model optimisation

The wax thickness (δw) was optimized using two distinct modeling approaches: The Response Surface Methodology (RSM) combined with desirability factors (DF), and the Artificial Neural Network (ANN) coupled with a Genetic Algorithm (GA). These two optimization strategies were implemented to identify the operating conditions that minimize wax deposition while maintaining realistic flow and thermodynamic constraints.

For the RSM optimization, the built-in numerical optimization algorithm in Design-Expert software was employed. The optimization was guided by the defined desirability functions, where wax thickness (δw) was set as the response to be minimized, while the input parameters—flow velocity (Vf), pressure (P), temperature difference (ΔT), wax appearance

temperature (TWAT), wax content (Wc), oil viscosity (μo), and asphaltene content (Ac)—were optimized within their respective experimental ranges. The desirability-based optimization produced multiple candidate solutions, from which the most desirable point was selected based on the highest composite desirability value. In parallel, the ANN–GA hybrid optimization was conducted using the MATLAB GA toolbox, where the trained ANN model served as the fitness function for the genetic algorithm. The GA iteratively adjusted the input parameters to minimize the predicted wax thickness, leveraging the ANN's nonlinear predictive capability and GA's global search efficiency. The combination of both methods provided a robust comparative framework—RSM–DF for statistically driven optimization and ANN–GA for intelligent global search—to identify the most favorable operating conditions for minimizing wax deposition.

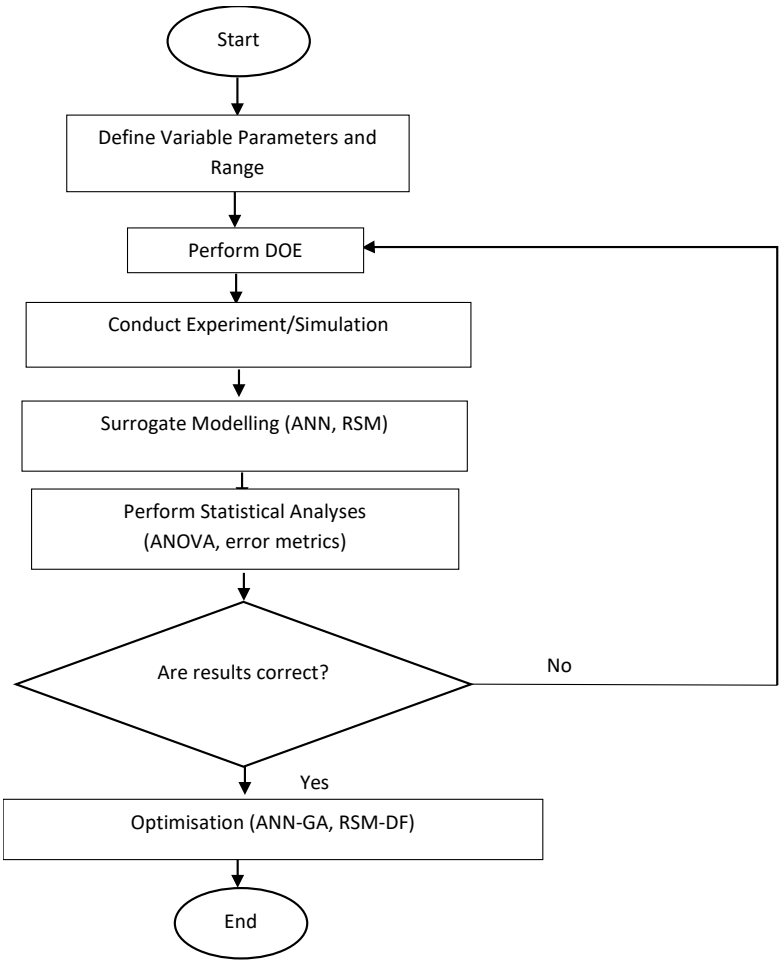


Figure 2. Flowchart of surrogate modelling and optimization.

### 3.5. Model performance metrics

Several statistical performance metrics were employed to evaluate the predictive accuracy of the developed RSM and ANN models. These include the coefficient of determination ($R^2$), mean squared error (MSE), root mean squared error (RMSE), mean absolute error (MAE), mean absolute percentage error (MAPE), and standard deviation (SD). The mathematical expressions for these evaluation parameters are presented below.

$$R^2 = \frac{\sum_{i=1}^{n}\left(x_{a,i} - x_{p,i}\right)^2}{\sum_{i=1}^{n}\left(x_{p,i} - x_{a,ave}\right)^2} \quad (18)$$

$$MSE = \frac{1}{n}\sum_{i=1}^{n}\left(x_{p,i} - x_{a,i}\right)^2 \quad (19)$$

$$RMSE = \sqrt{\frac{1}{n}\sum_{i=1}^{n}\left(x_{p,i} - x_{a,i}\right)^2} \quad (20)$$

$$MAE = \frac{1}{n}\sum_{i=1}^{n}\left|\left(x_{a,i} - x_{p,i}\right)\right| \quad (21)$$

$$MAPE = \frac{\frac{1}{n}\sum_{i=1}^{n}\left|\left(x_{a,i} - x_{p,i}\right)\right|}{\frac{1}{n}\sum_{i=1}^{n} x_{a,i}} \quad (22)$$

$$std\ dev = \sum_{i=1}^{n}\frac{(x_{di} - m)^2}{n-1} \quad (23)$$

where n is the number of experimental runs; xp,i is the estimated values; xa,i is the experimental values; xa,ave is the average experimental values; $x_{di}$ is the difference between the actual and estimated value; m is the mean value of $x_d$ dataset; k is the number of input variables.

## 4. Results and discussion

### 4.1. Results for ANN modelling

The ANN model result shown in Figure 3 displays the regression plots of ANN training, validation and testing for MLP-LM and MLP-BR. Figure 3a shows the result for MLP-LM while figure 3b shows that for MLP-BR.

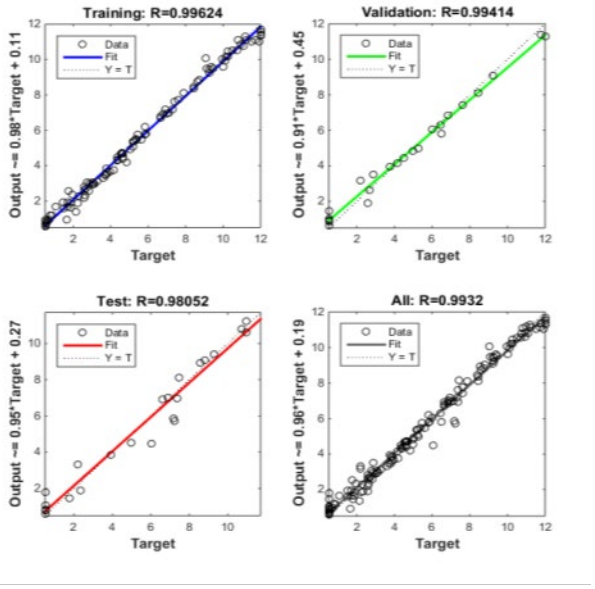


Figure 3a. R values for MLP-LM.

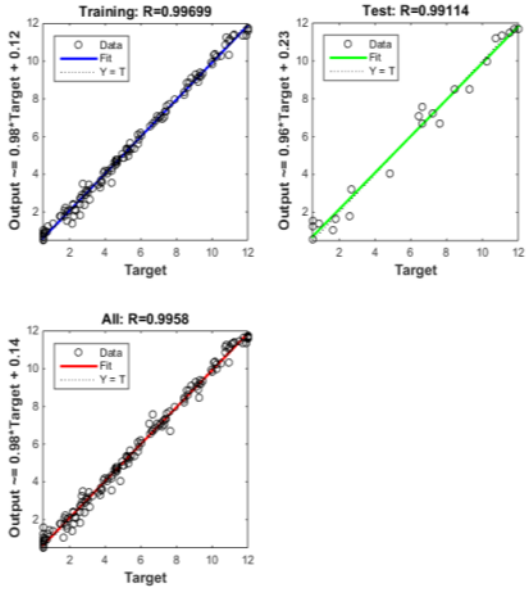


Figure 3b. R values for MLP-BR.

Figure 3 presents the correlation coefficients (R-values) for the two ANN models trained using the MLP-LM and MLP-BR algorithms. Both training algorithms achieved exceptionally high R-values, exceeding 0.99, which indicates a very strong correlation between the predicted and experimental wax thickness values. Specifically, the MLP-BR model exhibited a slightly higher R-value of 0.9958 compared to 0.9932 for the MLP-LM model, suggesting that the Bayesian Regularization algorithm achieved better generalization and fitting accuracy. This superior performance is attributed to BR's ability to automatically regulate the network's complexity during training, minimizing overfitting while maintaining high predictive precision. The

high R-values for both models confirm that the ANN architectures effectively captured the nonlinear relationships among the process variables governing wax deposition, with MLP-BR demonstrating marginally improved robustness and reliability.The performance plots of the ANN trainings are given in Figure 4.

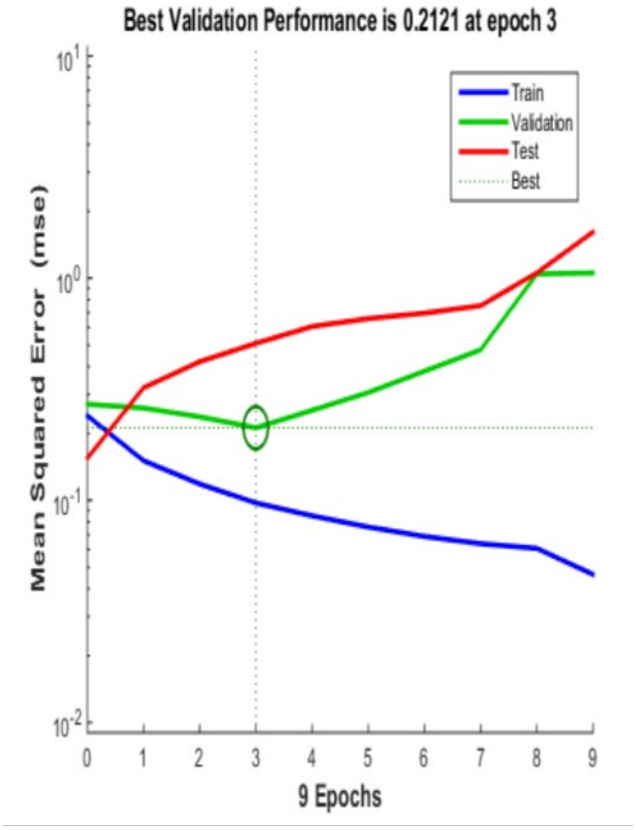


Figure 4a. MSE values for MLP-LM

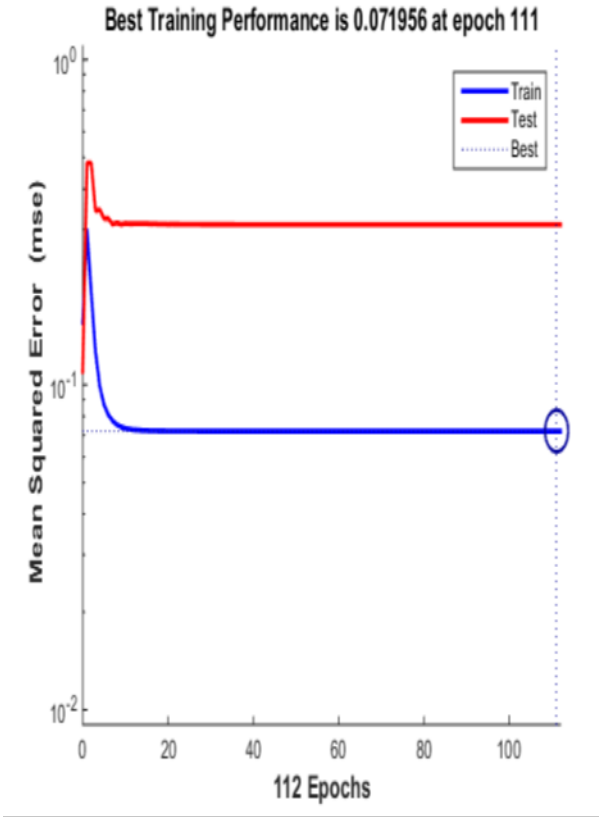


Figure 4b. MSE values for MLP-BR

The performance plots presented in Figure 3 illustrate the mean squared error (MSE) evolution during the training of the two multilayer perceptron (MLP) architectures—MLP-LM (Figure 4a) and MLP-BR (Figure 4b). Both networks demonstrate effective convergence, indicated by a consistent reduction in MSE as the training progresses. For the MLP-LM model, convergence was achieved after 9 epochs, with the minimum validation error of 0.2121 observed at epoch 3, beyond which further iterations did not significantly improve performance, suggesting early stabilization and prevention of overfitting through optimal weight adjustment. Conversely, the MLP-BR model exhibited a more gradual learning process, converging after 112 epochs, with the lowest validation MSE of 0.071956 recorded at epoch 111.

The notably lower MSE and extended training duration of the MLP-BR indicate its superior generalization capability and robustness, as the Bayesian Regularization algorithm inherently minimizes overfitting by incorporating a regularization term that balances the network's complexity and predictive accuracy. This contrasts with the Levenberg–Marquardt (LM) algorithm, which typically converges faster but may yield slightly higher residual errors when dealing with noisy or highly nonlinear datasets. Hence, while both models successfully captured the nonlinear relationships between the input parameters and wax deposition thickness, the MLP-BR architecture demonstrated a more stable and accurate learning performance, making it better suited for predictive modeling of complex, multivariate wax deposition behavior.

### 4.2. Results for RSM modelling

The RSM model results demonstrate the relationship between the independent process variables — flow velocity (Vf, m/s), pressure (P, MPa), temperature difference (ΔT, °C), wax appearance temperature (WAT, °C), water cut (Wc, %), crude oil viscosity (μo, cP), and asphaltene content (Ac, %) — and their collective influence on the wax layer thickness (δw, mm).Among the regression models evaluated, the Two-Factor Interaction (2FI) model provided the best fit to the experimental data (see Table 1), exhibiting the highest predictive accuracy and statistical significance. This model effectively captures the nonlinear interactions between key operational and compositional parameters influencing wax deposition in multiphase flow systems.The RSM-derived model (equation 24) mathematically represents the predictive relationship between the seven independent variables and the resulting wax deposition thickness, enabling quantitative evaluation of how process adjustments — such as reducing ΔT, optimizing flow velocity, or modifying oil composition — affect wax buildup under varying production conditions. This model thus serves as a valuable analytical tool for optimizing flow assurance strategies and mitigating wax formation in crude oil transport pipelines.

$$\textit{Wax Deposition}\ (mm) = 5.6969 - 2.8498A - 0.186445\,B + 3.10728C - 0.0178939D + 3.02636E + 1.96101F - 1.10973G - 0.143733AB - 0.444702AC + 0.0866813AD - 0.502335AE - 0.925202AF + 0.0519625AG + 0.162116BC + 0.0671215\,BD - 0.274041BE - 0.0304305BF + 0.0384699BG - 0.0431437CD + 0.363462\,CE + 0.335471CF - 0.0780947CG - 0.078076DE + 0.060703DF + 0.391363DG + 0.35808EF - 0.178346EG - 0.436057FG \quad (24)$$

For Equations (24), the variables A, B, C, D, E, F, and G correspond to the seven key process parameters influencing wax deposition: flow velocity (A: Vf, m/s), pressure (B: P, MPa), temperature difference (C: ΔT, °C), wax appearance temperature (D: WAT, °C), water cut (E: Wc, %), crude oil viscosity (F: μo, cP), and asphaltene content (G: Ac, %). These equations are employed to predict the response — wax layer thickness (δw, mm) — at specified levels of each input variable. To ensure accurate predictions, all factor levels must be expressed in their original physical units for both the input parameters and the output response. This allows for precise quantitative interpretation and comparison with experimental or field data. To evaluate the statistical robustness and relative influence of each factor and their interactions, an Analysis of Variance (ANOVA) was conducted. The results, summarized in Table 2, include key statistical metrics such as degrees of freedom (DF), mean square (MS), F-values, and p-values for the model and its terms. In Table 2, the p-values (< 0.0001) and the corresponding high F-values confirm that the regression model is highly significant, indicating that variations in the selected input parameters have a strong and measurable effect on wax deposition thickness. This validates the reliability of the developed RSM-based predictive model for assessing and optimizing wax deposition behavior under varying flow and compositional conditions.

Table 1. Error data for RSM model analyses.

| Source | Sequential p-value | Lack of Fit p-value | Adjusted $R^2$ | Predicted $R^2$ | |
|---|---|---|---|---|---|
| Linear | < 0.0001 | | 0.9591 | 0.9561 | |
| **2FI** | **< 0.0001** | | **0.972** | **0.9641** | **Suggested** |
| Quadratic | 0.5932 | | 0.9716 | 0.9612 | |
| Cubic | 0.2096 | | 0.9768 | 0.8481 | |
| Quartic | | | | | **Aliased** |

Table 2: RSM ANOVA

| Source | Sum of squares | df | Mean square | F-value | p-value | |
|---|---|---|---|---|---|---|
| Model | 1849.57 | 28 | 66.06 | 185.58 | < 0.0001 | significant |
| A-Flow velocity | 296.04 | 1 | 296.04 | 831.71 | < 0.0001 | |
| B-Pressure | 1.37 | 1 | 1.37 | 3.86 | 0.0518 | |
| C-ΔT | 430.27 | 1 | 430.27 | 1208.82 | < 0.0001 | |
| D-WAT | 0.0146 | 1 | 0.0146 | 0.0409 | 0.84 | |
| E-Wax content | 370.01 | 1 | 370.01 | 1039.5 | < 0.0001 | |
| F-Viscosity | 137.53 | 1 | 137.53 | 386.39 | < 0.0001 | |
| G-Asphaltene content | 55.49 | 1 | 55.49 | 155.88 | < 0.0001 | |
| AB | 0.2901 | 1 | 0.2901 | 0.8149 | 0.3685 | |
| AC | 3.69 | 1 | 3.69 | 10.36 | 0.0017 | |
| AD | 0.1125 | 1 | 0.1125 | 0.3161 | 0.575 | |
| AE | 3.4 | 1 | 3.4 | 9.55 | 0.0025 | |
| AF | 10.07 | 1 | 10.07 | 28.3 | < 0.0001 | |
| AG | 0.0389 | 1 | 0.0389 | 0.1092 | 0.7416 | |
| BC | 0.4296 | 1 | 0.4296 | 1.21 | 0.2741 | |
| BD | 0.0651 | 1 | 0.0651 | 0.1829 | 0.6697 | |
| BE | 0.958 | 1 | 0.958 | 2.69 | 0.1035 | |
| BF | 0.0122 | 1 | 0.0122 | 0.0342 | 0.8535 | |
| BG | 0.0216 | 1 | 0.0216 | 0.0606 | 0.806 | |
| CD | 0.0305 | 1 | 0.0305 | 0.0857 | 0.7702 | |
| CE | 1.6 | 1 | 1.6 | 4.5 | 0.036 | |
| CF | 1.51 | 1 | 1.51 | 4.26 | 0.0413 | |
| CG | 0.1028 | 1 | 0.1028 | 0.2889 | 0.5919 | |
| DE | 0.0875 | 1 | 0.0875 | 0.2457 | 0.621 | |
| DF | 0.056 | 1 | 0.056 | 0.1574 | 0.6922 | |
| DG | 2.45 | 1 | 2.45 | 6.88 | 0.0098 | |
| EF | 1.61 | 1 | 1.61 | 4.53 | 0.0353 | |
| EG | 0.3798 | 1 | 0.3798 | 1.07 | 0.3037 | |
| FG | 2.66 | 1 | 2.66 | 7.47 | 0.0072 | |
| Residual | 43.07 | 121 | 0.3559 | | | |
| Cor total | 1892.64 | 149 | | | | |

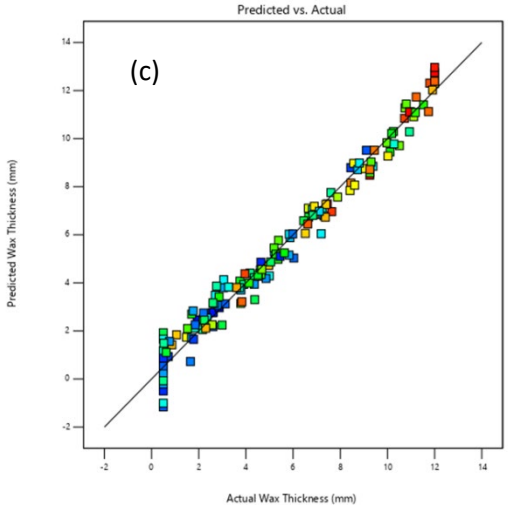


Figure 5. Parity plot of actual vs predicted values for wax thickness.

Figure 5 shows the actual vs. predicted response for the 2FI regression model.

Figure 5 depict parity plots illustrating the relationship between the actual and predicted responses for thickness. These figure demonstrate that the actual and predicted output responses closely align around the 45-degree line for all selected models, indicating strong regression and agreement between the two datasets. Thus, there exists an acceptable level of agreement between the actual experimental data and the predicted responses from the RSM models.

### 4.3 General performance metrics

Table 3 shows the comparison of performance metrics for the RSM and the ANN modelling. The comparative performance metrics for the MLP-LM, MLP-BR, and RSM models given in Table 3reveal clear distinctions in their predictive capabilities for modeling wax deposition behavior. Among the three models, the MLP-BR architecture achieved the most accurate and consistent predictions, as evidenced by its lowest mean squared error (MSE = 0.1073) and root mean squared error (RMSE = 0.3275), alongside the highest coefficient of determination ($R^2$ = 0.9918). This indicates that the Bayesian Regularization network captured nearly all the variance between the experimental and predicted wax thickness values, achieving superior generalization with minimal overfitting. The Levenberg–Marquardt (MLP-LM) model also performed strongly, with MSE = 0.1781, RMSE = 0.4220, and $R^2$ = 0.9864, showing that it could approximate the nonlinear relationships among the input variables with high precision, though slightly less effectively than MLP-BR. This marginal difference can be attributed to the inherent differences in training algorithms—while LM converges faster and efficiently minimizes local error, BR introduces an adaptive regularization term that balances model complexity with fitting accuracy, making it more resilient to noise and data variability typical of experimental wax deposition datasets.

Table 3. Performance metrics for RSM and ANN predictions.

| Metric | MLP-LM | MLP-BR | RSM |
|---|---|---|---|
| MSE | 0.178097 | 0.107268 | 0.287253 |
| RMSE | 0.422015 | 0.327518 | 0.53596 |
| MAE | 0.299648 | 0.239721 | 0.421105 |
| MAPE | 0.154478 | 0.123596 | 0.252083 |
| R2 | 0.98644 | 0.99175 | 0.97723 |

The RSM model, although demonstrating reasonable predictive ability with $R^2$ = 0.9772, was comparatively less accurate than the ANN-based models. Its MSE (0.2873), RMSE (0.5360), and MAE (0.4211) were higher, indicating greater deviation between predicted and actual wax deposition values. This outcome aligns with the inherent limitation of RSM as a second-order polynomial-based statistical approach, which assumes smooth, continuous response surfaces and may not fully capture the strong nonlinearities and complex interdependencies among parameters such as temperature differential, viscosity, and asphaltene content. In contrast, the ANN models—particularly MLP-BR—excel at representing such nonlinear, multivariable interactions due to their distributed learning and nonparametric structure.

Overall, these results demonstrate that ANN-based surrogate models significantly outperform RSM models in accurately predicting wax deposition trends under varying flow and thermodynamic conditions. The superior performance of MLP-BR further highlights the advantage of incorporating Bayesian Regularization in training neural networks for complex flow assurance problems, offering improved generalization and stability. Nonetheless, the RSM model remains valuable for providing interpretable parametric relationships and initial screening of key factors, while ANN models offer superior predictive power for dynamic and nonlinear wax deposition modeling.

### 4.4. Model optimisation

Table 4 presents the optimization results of the wax deposition modeling conducted using two advanced surrogate-based optimization techniques—Response Surface Methodology integrated with Desirability Function (RSM-DF) and Artificial Neural Network coupled with Genetic Algorithm (ANN-GA). The ANN-GA framework includes two ANN architectures, namely MLP-LM and MLP-BR, each trained and optimized separately to capture and minimize the wax layer thickness (δw, mm) under realistic flow and fluid property constraints. Both optimization strategies were designed to identify the most favorable operating conditions that minimize wax deposition while maintaining stable flow characteristics and crude oil properties. The seven independent variables considered were flow velocity (Vf), pressure (P), temperature difference

(ΔT), wax appearance temperature (WAT), water cut (Wc), oil viscosity (μo), and asphaltene content (Ac). The RSM-DF method employed a multi-objective desirability approach to generate several potential optimal points, with the best point determined by the highest composite desirability value (approaching 1.0), representing the most efficient condition for minimizing δw.

In parallel, the ANN-GA optimization was performed by coupling the predictive ANN models (MLP-LM and MLP-BR) with a Genetic Algorithm to achieve global optimization. The results demonstrate that the ANN-GA framework yielded lower optimal wax thickness values compared to RSM-DF, confirming its superior ability to capture nonlinear interactions among the process parameters and identify the true global optimum. Between the two ANN-GA configurations, the MLP-BR-GA exhibited the best performance, achieving the minimum δw value due to its enhanced generalization capability and robust learning characteristics. Overall, Table 8 provides a comprehensive summary of the optimization outcomes, illustrating how the integrated use of RSM-DF and ANN-GA (MLP-LM and MLP-BR) frameworks enables accurate identification of the optimal operating envelope for minimizing wax buildup. These results offer valuable insights for developing predictive control and flow assurance strategies in crude oil transport systems, supporting proactive wax management through data-driven optimization.

Table 4. Optimisation results.

| Parameter | Symbol | Unit | RSM | MLP-LM | MLP-BR |
|---|---|---|---|---|---|
| Flow velocity | Vf | m/s | 2.05 | 2.967 | 2.025 |
| Pressure | P | MPa | 13.73 | 3.061 | 3.041 |
| Temperature difference | ΔT | °C | 11.88 | 5.379 | 5.243 |
| Wax appearance temperature | TWAT | °C | 25.73 | 25.227 | 25.222 |
| Wax content | Wc | wt% | 1.29 | 1.281 | 1.280 |
| Oil viscosity | μo | cP | 16.46 | 2.454 | 2.43 |
| Asphaltene content | Ac | wt% | 0.24 | 0.231 | 0.230 |
| Wax thickness (output) | δw | mm | 0.385 | 0.227 | 0.223 |

The optimization of wax deposition parameters using RSM integrated with Desirability Functions (RSM-DF) generated multiple feasible solutions that satisfied the defined optimization objectives to varying degrees. From nearly one hundred computed optimal points, the most technically suitable and statistically consistent condition was selected based on both model accuracy and physicochemical relevance. The selected optimal condition (Table 4) corresponds to a flow velocity (Vf) of 2.05 m/s, pressure (P) of 13.73 MPa, temperature difference (ΔT) of 11.88 °C, wax appearance temperature (TWAT) of 25.73 °C, wax content (Wc) of 1.29 wt%, oil viscosity (μo) of 16.46 cP, and asphaltene content (Ac) of 0.24 wt%, resulting in a predicted wax layer thickness (δw) of 0.385 mm and a composite desirability value of 1.00. This optimal setting represents a balanced interaction between thermodynamic and hydrodynamic effects—where a moderate flow velocity maintains turbulent flow to suppress deposition, and a controlled temperature gradient limits wax crystallization and growth.

A comparative analysis of optimization outcomes from RSM-DF and Artificial Neural Network–Genetic Algorithm (ANN-GA) approaches (Table 4) highlights significant differences in predictive performance and solution quality. While RSM-DF successfully identified operating conditions that reduce wax accumulation, its quadratic polynomial structure inherently limits the accurate representation of nonlinear interactions among variables such as viscosity, flow rate, and temperature differential. Consequently, the RSM-derived optimum (δw = 0.385 mm) reflects a local minimum rather than a true global optimum in the complex multidimensional space of wax deposition behavior.

In contrast, the ANN-GA hybrid models, integrating Multilayer Perceptron (MLP) architectures with Levenberg–Marquardt (LM) and Bayesian Regularization (BR) training algorithms, achieved significantly improved results. The MLP-LM-GA and MLP-BR-GA frameworks yielded minimum wax thickness values of 0.227 mm and 0.223 mm, respectively. The superior performance of the ANN-GA models arises from their enhanced nonlinear learning capability and the global search efficiency of the genetic algorithm, which jointly enable accurate mapping and optimization of the complex relationships governing wax deposition.

The optimized parameter ranges identified by ANN-GA—pressure ≈ 3 MPa, temperature difference ≈ 5 °C, oil viscosity ≈ 2.4 cP, TWAT ≈ 25 °C, and Wc ≈ 1.28 %—demonstrate that reduced pressure, lower viscosity, and moderate temperature gradients favor minimal wax buildup. These trends align with established flow assurance principles emphasizing rheological control and thermal management for deposition mitigation.

Overall, the results confirm that ANN-GA provides a more accurate and robust optimization framework than RSM-DF for predicting and minimizing wax deposition. While RSM-DF remains valuable for preliminary parameter screening and for offering interpretable parametric trends, the MLP-BR-GA model proved to be the most effective surrogate optimization tool, combining strong generalization capability with high predictive precision in modeling the nonlinear behavior of wax formation systems.

## 5. Conclusion

This study developed and evaluated a hybrid surrogate intelligence framework integrating Response Surface Methodology (RSM) and Artificial Neural Networks (ANN) for the prediction and optimization of wax deposition in crude oil flow systems. The modeling approach employed seven governing parameters—flow velocity (Vf), pressure (P), temperature difference (ΔT), wax appearance temperature (TWAT), wax content (Wc), oil viscosity (μo), and asphaltene content (Ac)—to predict the resulting wax layer thickness (δw).

Within the RSM framework, a Custom Design configuration was implemented, and regression analysis indicated that the Two-Factor Interaction (2FI) model provided the best statistical fit among all tested models. The 2FI model achieved high predictive accuracy with $R^2$ = 0.972 and Predicted $R^2$ = 0.964, effectively capturing significant interaction effects such as flow velocity–ΔT, ΔT–viscosity, and viscosity–asphaltene content. The Analysis of Variance (ANOVA) confirmed the strong statistical significance of ΔT, Wc, and μo ($p < 0.0001$), underscoring their dominant influence on wax formation. The RSM–Desirability Function (RSM-DF) optimization yielded an optimal operating condition characterized by Vf = 2.05 m/s, P = 13.73 MPa, ΔT = 11.88 °C, TWAT = 25.73 °C, Wc = 1.29 wt%, μo = 16.46 cP, and Ac = 0.24 wt%, resulting in a predicted wax thickness (δw) of 0.385 mm with a composite desirability of 1.00.

In contrast, the ANN models—developed using Multilayer Perceptron (MLP) architectures trained with Levenberg–Marquardt (LM) and Bayesian Regularization (BR) algorithms—demonstrated markedly superior predictive and optimization performance. The MLP-BR model achieved the best overall accuracy with $R^2$ = 0.9918, RMSE = 0.3275, and MAPE = 0.1236, outperforming both MLP-LM and RSM models. When coupled with a Genetic Algorithm (GA) for optimization, the MLP-BR-GA and MLP-LM-GA configurations yielded minimum wax thicknesses of 0.223 mm and 0.227 mm, respectively—representing a 42–43% reduction relative to the RSM-DF optimum. The ANN-GA results further indicated that lower pressure (~3 MPa), reduced viscosity (~2.4 cP), and moderate temperature gradients (~5 °C) favor minimal wax deposition, aligning well with established flow assurance principles.

Overall, the comparative results confirm that the ANN-GA hybrid framework offers a more robust and accurate predictive capability for modeling complex nonlinear behaviors governing wax deposition, whereas the RSM-2FI model remains valuable for preliminary screening and interpretation of key parameter interactions. The integration of these complementary surrogate modeling techniques thus provides both explainability and precision, establishing a reliable data-driven approach for proactive wax management. The developed MLP-BR-GA model represents the most effective surrogate optimization tool for minimizing wax buildup, providing a strong foundation for intelligent flow assurance systems capable of real-time prediction and operational optimization in crude oil production environments.

**Appendix**

**Table A1: Training data and outputs**

| Flow Velocity (m/s) | Pressure (MPa) | ΔT (°C) | WAT (°C) | Wax content (%wt) | Oil viscosity (cP) | Asphaltene content (%wt) | Wax thickness (mm) | | | |
|---|---|---|---|---|---|---|---|---|---|---|
| 1.43635 | 13.89919 | 6.80886 | 40.54294 | 3.365091 | 13.45601 | 0.782082 | Actual | MLP-LM | MLP-BR | RSM |
| 2.876786 | 5.874743 | 23.59741 | 36.16808 | 4.900265 | 94.10355 | 0.27429 | 0.5 | 0.879231 | 0.869236 | 0.4044 |
| 2.329985 | 4.738738 | 23.92223 | 33.48444 | 3.478147 | 63.51539 | 0.708019 | 4.996136 | 4.830325 | 4.837347 | 4.29 |
| 1.996646 | 8.873433 | 27.31005 | 43.12709 | 2.241835 | 34.82075 | 1.832516 | 3.049267 | 3.065985 | 2.991799 | 3.8 |
| 0.890047 | 14.82781 | 30.4132 | 27.22395 | 2.688902 | 15.64866 | 1.379989 | 2.57101 | 2.191347 | 2.001494 | 2.77 |
| 0.889986 | 5.904663 | 39.15482 | 34.8525 | 7.450903 | 79.81447 | 2.699481 | 6.029865 | 4.468665 | 5.960845 | 5.03 |
| 0.645209 | 11.06563 | 23.07051 | 25.22707 | 3.888672 | 62.76713 | 2.488842 | 10.98117 | 11.21547 | 11.10603 | 11.12 |
| 2.66544 | 12.13944 | 16.30348 | 34.37321 | 6.099778 | 54.27919 | 1.157089 | 5.869948 | 5.82306 | 5.903145 | 5.88 |
| 2.002788 | 5.851651 | 32.83152 | 26.12607 | 8.047842 | 89.60147 | 0.926386 | 2.161964 | 1.380383 | 1.276882 | 2.05 |
| 2.270181 | 11.7386 | 14.47913 | 27.37636 | 10.66553 | 79.28253 | 1.263139 | 10.11201 | 9.955237 | 10.25304 | 9.45 |
| 0.551461 | 7.413398 | 20.364 | 27.35052 | 1.55037 | 16.86414 | 1.852826 | 5.245321 | 5.36921 | 6.269614 | 5.14 |
| 2.924775 | 10.58767 | 7.745973 | 37.98421 | 12.19175 | 32.54876 | 0.950578 | 2.620185 | 2.33934 | 2.759922 | 2.77 |
| 2.581107 | 10.60236 | 5.887276 | 39.9209 | 9.790605 | 26.35194 | 1.947617 | 1.059214 | 1.662457 | 1.250597 | 1.84 |
| 1.030848 | 9.429296 | 38.69269 | 36.66738 | 2.144626 | 74.90674 | 1.346353 | 0.5 | 1.054482 | 0.747766 | 0.79 |
| 0.954562 | 4.083477 | 34.2593 | 44.24345 | 13.2301 | 5.286179 | 1.745732 | 8.442661 | 8.086697 | 8.567451 | 8.79 |
| 0.958511 | 13.02363 | 29.3591 | 32.49741 | 13.89221 | 57.84919 | 1.421154 | 9.446158 | 9.507898 | 9.507509 | 9.52 |
| 1.260606 | 6.849361 | 19.31335 | 30.71424 | 1.855091 | 76.72095 | 1.024504 | 11.79329 | 11.38482 | 11.60739 | 12.31 |
| 1.811891 | 5.238222 | 11.0653 | 42.37198 | 4.876287 | 87.92303 | 2.855669 | 4.637804 | 4.495645 | 4.803568 | 4.86 |
| 1.579863 | 3.489302 | 10.4753 | 29.47192 | 12.28682 | 35.52401 | 2.338096 | 2.3502 | 1.899066 | 2.086384 | 2.54 |
| 1.228073 | 10.09072 | 13.7585 | 44.26445 | 11.47564 | 82.48322 | 0.592317 | 4.969786 | 4.543996 | 4.894846 | 4.73 |
| 2.029632 | 11.13077 | 24.22293 | 25.24309 | 3.583294 | 12.84191 | 2.63171 | 8.570466 | 8.934495 | 8.894145 | 8.97 |
| 0.848735 | 3.199054 | 30.01086 | 44.39758 | 3.930891 | 84.95232 | 1.564807 | 0.591042 | 0.763171 | 0.927809 | 1.37 |
| 1.230362 | 9.145117 | 28.10691 | 25.8632 | 6.186609 | 14.49389 | 2.704746 | 8.734556 | 8.842121 | 8.800946 | 8.71 |
| 1.415905 | 5.717949 | 14.79769 | 42.82286 | 7.783322 | 40.93415 | 2.439595 | 4.174948 | 3.764113 | 3.986026 | 4.41 |
| 1.640175 | 10.74207 | 38.42028 | 35.55402 | 9.655567 | 80.13495 | 1.390598 | 3.743878 | 3.945359 | 3.528747 | 4.07 |
| 2.46294 | 5.092397 | 30.82639 | 44.8593 | 6.164791 | 16.69191 | 0.262914 | 10.74431 | 10.80462 | 11.15372 | 11.28 |
| 0.999184 | 11.29125 | 24.40239 | 26.47593 | 7.475486 | 24.46664 | 0.952297 | 3.905793 | 3.830004 | 4.043881 | 3.93 |
| 1.785586 | 7.640824 | 26.41023 | 36.07709 | 11.46459 | 72.78075 | 1.716576 | 6.664981 | 6.783393 | 6.999232 | 6.74 |
| 1.981036 | 14.24076 | 19.686 | 44.38605 | 1.513565 | 72.56358 | 1.973739 | 9.062379 | 10.06694 | 9.274089 | 8.76 |

| Flow Velocity (m/s) | Pressure (MPa) | ΔT (°C) | WAT (°C) | Wax content (%wt) | Oil viscosity (cP) | Asphaltene content (%wt) | Wax thickness (mm) | | | |
|---|---|---|---|---|---|---|---|---|---|---|
| 0.616126 | 4.650251 | 13.67058 | 35.46196 | 4.534117 | 64.83247 | 0.922086 | 1.935164 | 2.358114 | 2.149209 | 2.45 |
| 2.018862 | 7.092796 | 17.45904 | 37.58797 | 10.98689 | 70.00695 | 0.590197 | 7.192466 | 5.849976 | 6.96647 | 6.04 |
| 0.92631 | 4.361682 | 31.52461 | 38.91497 | 13.5329 | 55.187 | 2.537805 | 6.64742 | 6.711714 | 7.139102 | 7.1 |
| 0.662629 | 14.09632 | 5.503772 | 34.09082 | 8.163484 | 26.67631 | 2.956326 | 11.2192 | 11.12982 | 11.33813 | 11.73 |
| 2.872214 | 13.52807 | 9.062542 | 37.55116 | 8.449589 | 35.87821 | 1.671933 | 2.183108 | 3.337091 | 2.373129 | 2.5 |
| 2.91408 | 6.0953 | 6.610092 | 36.68629 | 2.500408 | 19.79658 | 0.680702 | 0.5 | 1.024116 | 0.676979 | 0.4491 |
| 2.520993 | 10.91981 | 6.425508 | 43.02316 | 7.263773 | 91.02816 | 0.962461 | 0.5 | 0.76728 | 0.513753 | -1.16 |
| 1.261534 | 12.80667 | 34.94112 | 25.90893 | 8.456642 | 59.1724 | 0.251494 | 2.990452 | 2.886324 | 2.789681 | 2.24 |
| 0.74418 | 9.66241 | 29.62803 | 30.61926 | 4.394587 | 41.28344 | 2.760037 | 11.53039 | 11.03333 | 11.4106 | 11.41 |
| 2.210583 | 9.355807 | 21.59608 | 44.00823 | 4.769405 | 47.27657 | 0.529703 | 5.833217 | 6.213122 | 5.973468 | 6.02 |
| 1.600381 | 5.902227 | 8.424196 | 42.80528 | 6.281978 | 94.83377 | 1.814246 | 2.701351 | 2.702421 | 3.108581 | 3.49 |
| 0.805096 | 4.117233 | 22.20656 | 34.11314 | 1.280997 | 17.02844 | 0.967355 | 4.350874 | 4.498318 | 4.349004 | 4.21 |
| 1.737942 | 13.76659 | 21.57151 | 37.40265 | 5.509108 | 59.45052 | 1.751698 | 2.870497 | 2.982568 | 3.01817 | 2.96 |
| 0.585971 | 13.80502 | 11.06207 | 30.54762 | 3.960272 | 51.57709 | 2.023977 | 4.611634 | 4.737024 | 4.689142 | 4.54 |
| 2.773301 | 10.59722 | 20.18481 | 28.76242 | 5.584963 | 61.92252 | 2.523277 | 3.788755 | 3.836827 | 3.637758 | 3.71 |
| 1.14695 | 7.068357 | 18.94767 | 34.27397 | 2.67667 | 3.774798 | 0.77798 | 0.5 | 0.856903 | 1.133596 | 1.17 |
| 2.156306 | 7.190515 | 26.55475 | 32.06704 | 13.46738 | 87.46814 | 0.230788 | 2.600602 | 1.87442 | 1.605609 | 2.18 |
| 1.279278 | 11.71147 | 27.22828 | 36.67312 | 9.310294 | 93.34759 | 0.58328 | 11.74059 | 11.12365 | 11.34665 | 11.12 |
| 1.80017 | 13.76532 | 6.58564 | 26.55469 | 10.50743 | 57.38305 | 2.720052 | 10.79697 | 11.11654 | 11.17381 | 11.44 |
| 1.866776 | 13.64504 | 18.11144 | 44.4879 | 12.0484 | 70.27178 | 2.646892 | 2.569679 | 2.613525 | 2.412992 | 2.26 |
| 0.962136 | 12.35851 | 26.9051 | 44.72421 | 7.978191 | 92.40494 | 1.872757 | 6.518556 | 5.820074 | 6.572325 | 6.06 |
| 2.923962 | 10.70438 | 22.60977 | 38.96323 | 2.216884 | 71.30939 | 1.881447 | 10.25404 | 10.45577 | 10.22372 | 10.3 |
| 2.437832 | 4.00968 | 34.97714 | 35.72193 | 8.519492 | 16.94883 | 2.062103 | 0.710076 | 0.95751 | 0.934117 | 0.9334 |
| 2.848747 | 4.939545 | 28.05428 | 31.19055 | 9.215776 | 58.47626 | 0.69104 | 5.363456 | 5.488266 | 5.163787 | 4.98 |
| 2.737068 | 13.78265 | 10.7027 | 41.2759 | 11.43615 | 61.45807 | 2.760353 | 5.379383 | 5.461574 | 5.698702 | 5.77 |
| 1.99475 | 10.27715 | 7.469906 | 38.69462 | 7.043234 | 43.56481 | 1.372557 | 1.481419 | 1.931244 | 1.723772 | 1.74 |
| 2.804686 | 3.110365 | 27.48467 | 28.25234 | 2.786124 | 74.17154 | 1.272788 | 0.5 | 1.782671 | 1.14403 | 1.93 |
| 0.721231 | 4.217659 | 5.927896 | 43.21854 | 4.972863 | 93.56797 | 1.65297 | 2.203165 | 3.171588 | 2.611 | 2.74 |
| 0.989957 | 10.96202 | 25.50215 | 41.45074 | 6.083152 | 92.70571 | 0.331505 | 5.208392 | 5.087999 | 5.31796 | 5.29 |
| 0.613068 | 3.060739 | 37.90806 | 43.996 | 10.04284 | 46.18226 | 0.665593 | 10.93447 | 10.8619 | 10.35144 | 10.29 |
| 1.313326 | 4.929697 | 25.1416 | 39.51439 | 8.990896 | 13.09733 | 2.266494 | 12 | 11.70425 | 11.64924 | 12.66 |

| Flow Velocity (m/s) | Pressure (MPa) | ΔT (°C) | WAT (°C) | Wax content (%wt) | Oil viscosity (cP) | Asphaltene content (%wt) | Wax thickness (mm) | | | |
|---|---|---|---|---|---|---|---|---|---|---|
| 1.471693 | 9.584805 | 18.58595 | 37.2683 | 5.985354 | 98.51444 | 0.431836 | 5.194018 | 5.346914 | 5.344591 | 5.45 |
| 1.178373 | 11.30274 | 27.51509 | 33.36486 | 14.81121 | 84.21201 | 1.888826 | 7.602675 | 7.743622 | 7.62958 | 7.76 |
| 2.571844 | 10.82354 | 21.03885 | 43.65457 | 9.480847 | 14.21694 | 0.886978 | 12 | 11.30731 | 11.61079 | 12.75 |
| 1.391883 | 5.691232 | 24.09659 | 42.32128 | 4.321175 | 92.2425 | 1.290028 | 3.783316 | 3.477413 | 3.519111 | 3.15 |
| 1.202336 | 11.54615 | 37.95127 | 25.90437 | 2.424955 | 87.24984 | 1.008342 | 6.814865 | 6.924168 | 6.856546 | 7.04 |
| 1.85674 | 5.846989 | 18.51359 | 25.52734 | 3.140028 | 52.84613 | 1.195884 | 9.107989 | 9.499943 | 9.013545 | 9.51 |
| 0.852311 | 6.904796 | 38.64167 | 32.52927 | 4.443408 | 59.94499 | 2.213329 | 2.838562 | 2.556856 | 2.432003 | 3.07 |
| 2.505492 | 11.9579 | 36.68727 | 41.21107 | 3.249539 | 41.10226 | 1.031941 | 9.386794 | 9.614291 | 9.173282 | 8.85 |
| 0.686377 | 10.79559 | 11.85269 | 44.74552 | 3.611938 | 7.366641 | 1.785933 | 4.851407 | 4.181793 | 4.493966 | 4.18 |
| 2.967217 | 13.19068 | 7.427646 | 28.00834 | 4.991332 | 34.84933 | 1.532941 | 1.692115 | 1.667782 | 1.876186 | 1.71 |
| 2.430612 | 10.89135 | 8.52723 | 36.88261 | 3.42723 | 80.67964 | 2.058279 | 0.5 | 0.549047 | 0.531244 | -1.01 |
| 0.996789 | 9.819703 | 5.637764 | 32.61782 | 13.55472 | 2.453938 | 2.823123 | 0.5 | 0.616756 | 0.809562 | 0.2433 |
| 0.513805 | 4.124097 | 8.305504 | 44.39829 | 2.123272 | 34.68292 | 2.251202 | 3.831488 | 3.603663 | 3.163748 | 3.22 |
| 2.538654 | 7.41259 | 28.90524 | 41.84238 | 8.343159 | 41.02053 | 0.801833 | 1.781649 | 1.477785 | 1.784755 | 1.65 |
| 2.267143 | 6.182428 | 7.491603 | 41.76657 | 6.745556 | 54.66477 | 0.287313 | 5.26919 | 4.978641 | 5.155272 | 5.19 |
| 2.322518 | 5.927876 | 16.16415 | 34.37386 | 14.7533 | 92.14585 | 0.934339 | 2.239966 | 1.856024 | 1.734147 | 2.45 |
| 2.428176 | 14.67613 | 34.57064 | 33.29639 | 2.568545 | 35.94191 | 1.866218 | 9.247654 | 9.068285 | 9.166586 | 8.48 |
| 0.685112 | 7.717173 | 5.814518 | 30.46814 | 6.569978 | 36.00141 | 0.343992 | 3.12316 | 2.958712 | 2.988612 | 3.13 |
| 1.396164 | 13.70456 | 33.5064 | 26.12751 | 14.57259 | 74.27512 | 1.589825 | 4.584345 | 4.693802 | 4.675326 | 4.4 |
| 0.789673 | 10.57366 | 14.86492 | 42.29445 | 13.1171 | 46.31736 | 1.87116 | 12 | 11.55682 | 11.66911 | 12.96 |
| 2.657759 | 12.53774 | 9.135769 | 41.25802 | 12.43901 | 24.01127 | 1.135883 | 8.449648 | 8.365589 | 8.310554 | 8.15 |
| 2.058245 | 9.031645 | 29.3858 | 44.99435 | 4.61064 | 46.33907 | 2.358554 | 2.297374 | 2.293276 | 1.975703 | 2.11 |
| 1.327245 | 9.922847 | 27.013 | 44.93274 | 3.392426 | 15.80399 | 0.498475 | 3.058509 | 2.945483 | 3.92995 | 4.13 |
| 0.658896 | 8.910212 | 35.71152 | 36.10863 | 10.36101 | 19.28592 | 0.410386 | 4.356456 | 4.352933 | 4.373293 | 3.94 |
| 1.277456 | 5.342916 | 30.72749 | 40.37975 | 14.01126 | 50.84004 | 2.238929 | 11.11489 | 10.79486 | 11.21356 | 10.91 |
| 1.312958 | 11.66943 | 33.12183 | 43.89531 | 8.794681 | 43.05469 | 1.587376 | 10.72272 | 10.54877 | 10.80211 | 10.84 |
| 2.324015 | 6.369268 | 14.87121 | 41.99295 | 9.002578 | 91.6549 | 2.127527 | 9.261371 | 9.250297 | 9.248808 | 8.58 |
| 2.093894 | 3.291792 | 11.21038 | 29.94696 | 4.919707 | 37.5146 | 1.417517 | 4.641765 | 4.377003 | 4.624666 | 4.35 |
| 2.718032 | 10.74567 | 31.27152 | 34.01088 | 11.7729 | 58.89766 | 0.889926 | 0.5 | 0.907871 | 0.82061 | 1.66 |
| 1.680537 | 5.125328 | 33.23922 | 27.58319 | 3.618612 | 63.9619 | 2.493486 | 6.898688 | 7.032794 | 7.366768 | 7.18 |
| 0.798986 | 14.2855 | 39.66768 | 44.08102 | 5.531509 | 3.283257 | 2.438364 | 5.832239 | 5.778069 | 5.833359 | 5.16 |

| Flow Velocity (m/s) | Pressure (MPa) | ΔT (°C) | WAT (°C) | Wax content (%wt) | Oil viscosity (cP) | Asphaltene content (%wt) | Wax thickness (mm) | | | |
|---|---|---|---|---|---|---|---|---|---|---|
| 2.283112 | 14.44714 | 19.44162 | 37.12349 | 6.95611 | 67.02666 | 2.14515 | 7.23804 | 5.695956 | 7.259661 | 6.99 |
| 2.401963 | 13.97837 | 18.02063 | 29.57286 | 8.106545 | 19.44752 | 0.962006 | 4.375439 | 4.297606 | 3.762456 | 3.3 |
| 1.903193 | 7.441904 | 32.17445 | 38.43401 | 4.393736 | 96.18489 | 1.852646 | 1.701375 | 1.940315 | 1.872983 | 2.7 |
| 2.427418 | 3.185479 | 16.92812 | 37.36256 | 2.607716 | 16.56895 | 1.210727 | 7.310479 | 7.185266 | 7.114683 | 6.79 |
| 1.734489 | 14.13982 | 37.57651 | 32.16325 | 9.548681 | 42.63316 | 0.45643 | 0.5 | 0.924333 | 0.624553 | 0.5451 |
| 1.806832 | 8.13821 | 35.04445 | 27.27115 | 5.040828 | 10.36427 | 2.768478 | 10.50866 | 10.54385 | 10.28103 | 9.71 |
| 1.568853 | 14.59986 | 20.01479 | 38.43146 | 9.137335 | 99.69368 | 0.583092 | 3.268006 | 3.093692 | 3.383277 | 3.83 |
| 0.563548 | 14.56344 | 31.28049 | 35.40615 | 3.161078 | 51.21511 | 2.860665 | 9.307215 | 9.422221 | 9.3471 | 9.03 |
| 0.769729 | 13.23611 | 31.409 | 40.44637 | 7.735961 | 60.34773 | 1.448816 | 7.003939 | 6.959549 | 6.964218 | 6.85 |
| 0.578573 | 6.533387 | 8.609335 | 35.40327 | 8.456252 | 8.573495 | 0.718372 | 10.1771 | 10.20479 | 10.43519 | 10.21 |
| 2.091026 | 7.621173 | 36.58935 | 42.04363 | 1.72553 | 75.49613 | 1.717323 | 4.134321 | 4.135935 | 3.956635 | 3.99 |
| 1.28589 | 13.21364 | 22.68383 | 36.03814 | 5.71246 | 22.57075 | 2.644248 | 5.451063 | 5.758395 | 5.392606 | 5.1 |
| 1.771427 | 6.803064 | 33.92601 | 36.21876 | 2.881805 | 90.00932 | 2.25023 | 3.728226 | 3.452322 | 3.399844 | 3.8 |
| 2.768916 | 5.033913 | 16.20174 | 42.53307 | 1.88725 | 22.10368 | 2.458371 | 5.984563 | 6.032217 | 6.328191 | 6.03 |
| 1.123231 | 9.681615 | 36.34331 | 33.06966 | 14.85944 | 20.6874 | 2.044593 | 0.5 | 0.585398 | 0.528106 | -0.4959 |
| 1.525957 | 14.23386 | 18.62206 | 27.6803 | 5.512954 | 5.581867 | 2.138374 | 10.93894 | 10.59715 | 11.06531 | 11.11 |
| 2.388878 | 11.35236 | 5.379318 | 25.57565 | 12.33824 | 48.26256 | 2.577748 | 1.831913 | 1.6289 | 1.524067 | 2.12 |
| 1.071995 | 9.840734 | 36.68837 | 40.10275 | 4.564969 | 57.35443 | 0.89907 | 0.862126 | 1.164781 | 1.228254 | 1.42 |
| 0.69245 | 4.166118 | 8.195034 | 37.40619 | 10.54104 | 8.439447 | 1.57039 | 8.809174 | 9.053498 | 9.141091 | 8.98 |
| 1.224379 | 10.38009 | 16.17598 | 39.0816 | 11.64319 | 78.00171 | 0.819386 | 4.532668 | 4.682343 | 4.502871 | 4.27 |
| 0.903053 | 14.88065 | 38.25217 | 29.25928 | 9.338942 | 46.42231 | 2.96547 | 10.02318 | 9.616021 | 9.77284 | 9.28 |
| 2.824244 | 4.681008 | 38.27125 | 27.72743 | 7.602067 | 53.39025 | 2.843366 | 9.978136 | 10.04455 | 9.833791 | 9.83 |
| 2.520301 | 9.219956 | 25.07033 | 25.29089 | 6.765773 | 45.19475 | 0.310395 | 4.511893 | 4.455147 | 4.557 | 4.33 |
| 2.083509 | 13.52848 | 27.1143 | 32.01175 | 5.884156 | 41.27478 | 2.17561 | 5.048199 | 4.924109 | 4.918513 | 4.87 |
| 2.678651 | 11.88922 | 20.69559 | 36.79835 | 14.01341 | 56.84475 | 2.790695 | 2.755409 | 3.052191 | 3.53959 | 3.86 |
| 2.50918 | 11.36419 | 15.26238 | 32.84488 | 12.62867 | 17.21354 | 0.705611 | 3.959472 | 3.644638 | 4.10692 | 4.38 |
| 0.966425 | 11.42981 | 16.50326 | 33.7495 | 14.51038 | 19.82896 | 1.790247 | 3.610056 | 3.316938 | 3.555701 | 3.81 |
| 2.731397 | 7.313894 | 28.53815 | 43.08317 | 2.740161 | 86.45499 | 2.763367 | 7.448001 | 8.13496 | 7.610018 | 7.29 |
| 1.848356 | 6.523102 | 31.33311 | 31.96511 | 11.23214 | 94.71932 | 0.295049 | 1.850655 | 1.860914 | 2.075597 | 2.26 |
| 2.5186 | 12.71233 | 32.70527 | 35.27979 | 14.13677 | 38.58431 | 2.152777 | 12 | 11.40111 | 11.66268 | 12.29 |
| 2.740228 | 12.72136 | 32.63663 | 40.67306 | 3.537263 | 28.53298 | 1.032577 | 7.64183 | 7.417016 | 6.671368 | 6.97 |

| Flow Velocity (m/s) | Pressure (MPa) | ΔT (°C) | WAT (°C) | Wax content (%wt) | Oil viscosity (cP) | Asphaltene content (%wt) | Wax thickness (mm) | | | |
|---|---|---|---|---|---|---|---|---|---|---|
| 1.295009 | 13.40487 | 8.192214 | 32.93086 | 1.930948 | 65.11196 | 2.788309 | 1.763936 | 2.546168 | 2.362861 | 2.84 |
| 0.77513 | 13.95889 | 22.30471 | 37.44173 | 11.37569 | 42.05595 | 2.918963 | 0.5 | 0.855938 | 1.05705 | 0.8659 |
| 1.069838 | 9.136109 | 7.014557 | 42.24727 | 9.042624 | 4.487863 | 2.843946 | 8.414818 | 8.464387 | 8.305523 | 7.84 |
| 1.567769 | 9.018196 | 24.23351 | 43.99041 | 12.7856 | 17.30295 | 1.5278 | 1.523965 | 1.577059 | 1.828605 | 2.1 |
| 2.545037 | 12.57954 | 20.45357 | 27.94147 | 2.956813 | 72.16528 | 2.613719 | 6.9134 | 7.201397 | 7.497226 | 6.85 |
| 2.651826 | 10.79957 | 36.06965 | 43.53175 | 12.13374 | 66.57455 | 2.564738 | 1.647135 | 0.93303 | 1.555357 | 0.7277 |
| 0.51738 | 11.4236 | 17.28203 | 34.84233 | 3.822782 | 4.655407 | 1.093481 | 7.393129 | 7.619035 | 7.409373 | 7.26 |
| 1.776868 | 12.54951 | 9.097346 | 30.16489 | 3.291183 | 23.75327 | 2.520963 | 2.669568 | 2.628096 | 2.672472 | 3.14 |
| 1.543528 | 13.68006 | 10.00471 | 34.18272 | 3.299721 | 24.64533 | 0.303621 | 0.5 | 0.646676 | 0.571066 | -0.2056 |
| 1.05527 | 7.055942 | 31.65287 | 44.60065 | 12.40405 | 67.84549 | 1.869556 | 0.75856 | 1.201025 | 1.181635 | 1.56 |
| 0.799663 | 7.506995 | 26.63763 | 34.85236 | 10.31276 | 3.931633 | 0.844025 | 11.91272 | 11.02396 | 11.3335 | 12.02 |
| 1.344038 | 4.127783 | 8.539294 | 31.57503 | 8.322916 | 12.20264 | 0.537587 | 7.885492 | 8.112814 | 7.831426 | 7.57 |
| 2.857274 | 9.939362 | 7.943738 | 37.66802 | 6.023627 | 80.39178 | 0.415469 | 2.865312 | 3.513917 | 3.063853 | 3.42 |
| 1.308007 | 3.431307 | 29.53392 | 29.80291 | 13.28081 | 19.49738 | 2.149609 | 0.518819 | 1.44571 | 1.305382 | 1.49 |
| 1.796977 | 8.587176 | 7.546705 | 26.51727 | 6.494232 | 65.96912 | 1.15165 | 9.254234 | 9.459239 | 9.30126 | 8.71 |
| 2.257547 | 9.511736 | 33.7651 | 27.57759 | 12.43239 | 25.34191 | 2.229347 | 2.600076 | 2.830042 | 2.634325 | 3.17 |
| 1.409074 | 6.438495 | 29.71848 | 27.56092 | 7.147889 | 11.74526 | 0.382998 | 7.367614 | 6.9589 | 7.338225 | 6.73 |
| 2.929455 | 10.09 | 7.847207 | 28.03805 | 6.277222 | 25.83087 | 1.082813 | 6.447182 | 6.295778 | 6.26035 | 6.59 |
| 2.906118 | 3.366003 | 7.96932 | 27.77654 | 7.477517 | 72.78216 | 1.710576 | 0.5 | 0.677156 | 0.541598 | -0.0716 |
| 1.129456 | 3.448178 | 39.53239 | 37.81749 | 5.21929 | 85.85825 | 2.414025 | 0.622858 | 0.852436 | 0.920525 | 1.11 |
| 1.743121 | 12.87121 | 18.09948 | 28.6376 | 11.46653 | 83.36155 | 1.092507 | 10.27803 | 10.19844 | 10.28494 | 9.78 |
| 1.252196 | 7.322288 | 17.97248 | 31.91335 | 8.038085 | 40.92399 | 1.952496 | 8.610791 | 8.734822 | 8.726797 | 8.07 |
| 1.212101 | 4.524726 | 33.44798 | 42.93577 | 4.250978 | 67.47234 | 2.680738 | 5.631827 | 5.477982 | 4.899955 | 5.25 |
| 0.592217 | 9.266919 | 38.1537 | 34.47923 | 13.59404 | 22.08846 | 1.924417 | 7.11212 | 6.978252 | 7.102731 | 6.97 |
| 2.023911 | 12.23992 | 39.51004 | 38.35115 | 6.374477 | 30.72848 | 0.852287 | 12 | 11.37778 | 11.57226 | 12.39 |
| 1.756698 | 5.589852 | 31.36824 | 28.4464 | 8.60974 | 89.84091 | 0.268322 | 6.839196 | 6.856746 | 6.897592 | 6.81 |
| 0.628697 | 10.47469 | 18.16909 | 28.84578 | 13.69061 | 3.274189 | 2.636277 | 11.18422 | 11.29852 | 11.22334 | 11.09 |
| 1.196616 | 4.02417 | 7.922525 | 25.81737 | 9.739332 | 10.37984 | 0.259554 | 6.623871 | 6.911623 | 6.543472 | 6.45 |

## References


[1] Li B, Guo Z, Zheng L, Qi B. A comprehensive review of wax deposition in crude oil systems: mechanisms, influencing factors, prediction and inhibition techniques. Fuel, 2024; 357: 129676. https://doi.org/10.1016/j.fuel.2023.129676

[2] Kiyingi W, Guo J-X, Xiong R-Y, Su L, Yang X-H, Zhang S-L. Crude oil wax: a review on formation, experimentation, thermodynamic and kinetic modeling, prediction and remediation techniques. Petroleum Science, 2022; 19: 2343–2357. https://doi.org/10.1016/j.petsci.2022.08.008

[3] Sousa AL, Matos HA, Guerreiro LP. Preventing and removing wax deposition inside vertical wells: a review. Journal of Petroleum Exploration & Production Technology, 2019; 9: 2091–2107. https://doi.org/10.1007/s13202-019-0609-x

[4] Wen J. Progress in wax deposition characteristics and prediction methods for high pour point and viscous crude oil water system. Processes, 2025; 13(4): 1115. https://doi.org/10.3390/pr13041115

[5] Elphingstone Jr GM, Greenhill KL, Hsu JJC. Modeling of multiphase wax deposition. Journal of Energy Resources Technology-transactions of The Asme, 1999;121: 81-85. https://doi.org/10.1115/1.2795072

[6] Elkatory MR. Mitigation and remediation technologies of waxy crude. Polymers, 2022; 14(16): 3231. https://doi.org/10.3390/polym14163231

[7] Amar MN, Singh S, Bahadur I, Hashemi H, Ramjugernath D. Predicting wax deposition using robust machine learning. Results in Engineering, 2022; 15: 100484. https://doi.org/10.1016/j.rineng.2022.100484.

[8] Zhu H, Yu P, Li C, Yang F, Yao B, Yang S, Peng H. Wax deposition during the transportation of waxy crude oil: modeling and field implications. Energy & Fuels, 2024, 38(5), 2319–2332. https://doi.org/10.1021/acs.energyfuels.3c04687

[9] Lal B, Bavoh CB, Sayani JKS Machine-learning in wax deposition: methodologies, numerical models, and artificial intelligence for flow assurance. In: Machine Learning and Flow Assurance in Oil and Gas, 2023, pp. 1–25.

[10] Khalighi J. et al. Wax precipitation prediction using a novel intelligent method based on LS-SVM and genetic algorithm. Journal of Petroleum Science & Engineering, 2024. https://doi.org/10.1016/j.petrol.2024.112376

[11] Ahmadi M. Data-driven approaches for predicting wax deposition. Energy, 2023, 265, 126296. https://doi.org/10.1016/j.energy.2022.126296

[12] Obanijesu EO, Omidiora EO. Artificial neural network's prediction of wax deposition potential of Nigerian crude oil for pipeline safety. Petroleum Science & Technology, 2008; 26(15–16): 1977–1991. https://doi.org/10.1080/10916460701399485

[13] Zhang Z, Shen Y, Zhang L, Xiao S, Jin X. A wax deposition prediction method for pumping oil wells based on LSTM neural networks. Journal of Engineering Science and Technology Review, 2023, 16(6), 177–184. https://doi.org/10.25103/jestr.166.22

[14] Ridzuan N, Yaacob Z, Adam FW. Response surface methodology on wax deposit optimization. Malaysian Journal of Analytical Sciences, 2017; 21(2): 452–459. https://doi.org/10.17576/mjas-2017-2102-21.

[15] Dehaghani AHS. An intelligent model for predicting wax deposition thickness during turbulent flow of oil. Petroleum Science and Technology, 2017; 35: 1706–1711. https://doi.org/10.1080/10916466.2017.1358281

[16] Alnaimat F, Ziauddin M. Wax deposition and prediction in petroleum pipelines. Journal of Petroleum Science and Engineering, 2020; 184: 106385. https://doi.org/10.1016/j.petrol.2019.106385.

[17] Eghtedaei R, Sasanipour J, Zarrabi H, Palizian M, Baghban A. Estimation of wax deposition in oil production units using an RBF-ANN strategy. Petroleum Science and Technology, 2017; 35: 1737–1742. https://doi.org/10.1080/10916466.2017.1380043

[18] Nait Amar M, Ghahfarokhi AJ, Ng CSW. Predicting wax deposition using robust machine learning techniques. Petroleum, 2022; 8(2): 167–173. https://doi.org/10.1016/j.petlm.2021.07.005.

[19] Xie Y, Xing Y. A prediction method for the wax deposition rate based on a radial basis function neural network. Petroleum, 2017; 3(2): 237–241. https://doi.org/10.1016/j.petlm.2016.11.003.

[20] Obibuike UJ, Ekwueme ST, Ohia NP, Ukaeru FC, Onyejekwe IM, Udechukwu MC, Yahya HB. Modelling and optimisation of geothermal binary ORC systems using response surface methodology and artificial neural networks. Zaštita Materijala, 2026; 67(1): 14-35. https://doi.org/10.62638/ZasMat1329.
[21] Jalalnezhad MJ, Kamali V. Development of an intelligent model for wax deposition in oil pipeline. Journal of Petroleum Exploration and Production Technology, 2016; 6(1): 129–133. https://doi.org/10.1007/s13202-015-0160-3.
[22] Kim D, Park H, Lee S, Cho J. AI-based prediction of wax deposition characteristics in crude oil pipelines using experimental and sensor data. Journal of Petroleum Science and Engineering, 2022; 213: 110520. https://doi.org/10.1016/j.petrol.2022.110520
[23] Chen Z. Modeling wax deposition rate in waxy crude oil pipelines using artificial neural networks. Energy Reports, 2024; 11: 458–470. https://doi.org/10.1016/j.egyr.2024.01.065.
[24] Jin W, Zhang L, Li Q, Liu G. Artificial neural network modeling for prediction of wax deposition thickness from experimental flow-loop data. Fuel, 2023; 346: 128249. https://doi.org/10.1016/j.fuel.2023.128249.
[25] Obaseki FA, Al-Majed A, Ahmed R. Dynamic modeling and ANN-assisted prediction of wax deposition in multiphase pipelines. Journal of Energy Resources Technology, 2021; 143(8): 083002. https://doi.org/10.1115/1.4050019.
[26] Shehata SA, El-Metwally IM, Abdelgawad KF, Elkhawaga FA. Efficacy of agro-industrial wastes on the weed control, nutrient uptake, growth, and yield of onion crop (*Allium cepa* L.). Journal of Soil Science and Plant Nutrition, 2022; 22(2): 2707–2718. https://doi.org/10.1007/s42729-022-00858-0.
[27] Khama ER, Loyibo EZ, Okologume W, Ekwueme ST, Okafor CV, Ohia NP. Investigation of the performance of activated carbon derived from ripe plantain peels for $CO_2$ capture: modelling and optimisation using response surface methodology. Zaštita Materijala, 2024, 65(2), 258–272. https://doi.org/10.62638/ZasMat1329
[28] Obibuike UJ, Ekwueme ST, Ohia NP, Ukaeru FC, Onyejekwe IM, Udechukwu MC, Yahya HB. Modelling of drillstring hook loads for torque and drag evaluation in extended reach wells. Petroleum & Coal, 2025; 67(2): 540.
[29] Salam KK, Arinkoola AO, Oke EO, Adeleye JO. Optimization of operating parameters using response surface methodology for paraffin-wax deposition in pipeline. Petroleum & Coal, 2014; 56(1): 19–28.
[30] Adeyanju OA, Oyekunle LO. Optimization of wax deposition in sub-cooled pipeline using response surface methodology. In: SPE Nigeria Annual International Conference and Exhibition, 2015, SPE-178275. Society of Petroleum Engineers. https://doi.org/10.2118/178275-MS.
[31] Elganidi I, Elarbe B, Ridzuan N, Abdullah N. Optimisation of reaction parameters for a novel polymeric additives as flow improvers of crude oil using response surface methodology. Journal of Petroleum Exploration and Production Technology, 2022; 12(2): 437–449. https://doi.org/10.1007/s13202-021-01254-9

*To whom correspondence should be addressed: Stanley Toochukwu Ekwueme , Department of Petroleum Engineering, FUTO Owerri, Nigeria, E-mail: stanleyekwueme@yahoo.com*